Defense Nuclear Agency
Alexandria, VA 22310-3398

DNA-TR-89-132

Theory and Verification of the Fiber Composite Damage Model Implemented in DYNA3D

Y. D. Murray
APTEK, Inc.
4320 Stevens Creek Blvd.
Suite 195
San Jose, CA 95129

December 1989

Technical Report

CONTRACT No. DNA 001-88-C-0040

Approved for public release;
distribution is unlimited.

Destroy this report when it is no longer needed. Do not return to sender.

PLEASE NOTIFY THE DEFENSE NUCLEAR AGENCY, ATTN: CSTI, 6801 TELEGRAPH ROAD, ALEXANDRIA, VA 22310-3398, IF YOUR ADDRESS IS INCORRECT, IF YOU WISH IT DELETED FROM THE DISTRIBUTION LIST, OR IF THE ADDRESSEE IS NO LONGER EMPLOYED BY YOUR ORGANIZATION.

DISTRIBUTION LIST UPDATE

This mailer is provided to enable DNA to maintain current distribution lists for reports. We would appreciate your providing the requested information.

☐ Add the individual listed to your distribution list.

☐ Delete the cited organization/individual.

☐ Change of address.

NAME: _____

ORGANIZATION: _____

OLD ADDRESS	CURRENT ADDRESS
_____	_____
_____	_____
_____	_____

TELEPHONE NUMBER: (___) _____

SUBJECT AREA(s) OF INTEREST:

_____ _____

_____ _____

_____ _____

DNA OR OTHER GOVERNMENT CONTRACT NUMBER: _____

CERTIFICATION OF NEED-TO-KNOW BY GOVERNMENT SPONSOR (if other than DNA):

SPONSORING ORGANIZATION: _____

CONTRACTING OFFICER OR REPRESENTATIVE: _____

SIGNATURE: _____

CUT HERE AND RETURN

REPORT DOCUMENTATION PAGE

1a REPORT SECURITY CLASSIFICATION UNCLASSIFIED	1b RESTRICTIVE MARKINGS
2a SECURITY CLASSIFICATION AUTHORITY N/A since Unclassified	3 DISTRIBUTION/AVAILABILITY OF REPORT Approved for public release; distribution is unlimited.
2b DECLASSIFICATION/DOWNGRADING SCHEDULE N/A since Unclassified	
4 PERFORMING ORGANIZATION REPORT NUMBER(S) A-89-4R	5 MONITORING ORGANIZATION REPORT NUMBER(S) DNA-TR-89-132
6a NAME OF PERFORMING ORGANIZATION APTEK, Inc. — 6b OFFICE SYMBOL (if applicable)	7a NAME OF MONITORING ORGANIZATION Defense Nuclear Agency
6c ADDRESS (City, State, and ZIP Code) 4320 Stevens Creek Blvd. Suite 195 San Jose, CA 95129	7b ADDRESS (City, State, and ZIP Code) 6801 Telegraph Road Alexandria, VA 22310-3398
8a NAME OF FUNDING/SPONSORING ORGANIZATION — 8b OFFICE SYMBOL (if applicable) SPWE/Frankel	9 PROCUREMENT INSTRUMENT IDENTIFICATION NUMBER DNA 001-88-C-0040
8c ADDRESS (City, State, and ZIP Code)	10 SOURCE OF FUNDING NUMBERS PROGRAM ELEMENT NO: 62715H — PROJECT NO: X — TASK NO: C — WORK UNIT ACCESSION NO: DH880040

11 TITLE (Include Security Classification)

Theory and Verification of the Fiber Composite Damage Model Implemented in DYNA3D

12 PERSONAL AUTHOR(S)
Murray, Yvonne D.

13a TYPE OF REPORT	13b TIME COVERED	14 DATE OF REPORT (Year, Month, Day)	15 PAGE COUNT
Technical	FROM 890111 TO 890601	891201	76

16 SUPPLEMENTARY NOTATION
This work was sponsored by the Defense Nuclear Agency under RDT&E RMC Codes B342085764 X C 00017 25904D and B342085764 X C 00018 25904D.

17 COSATI CODES			18 SUBJECT TERMS (Continue on reverse if necessary and identify by block number)		
FIELD	GROUP	SUB-GROUP			
20	11		Matrix Cracking	Composite	Failure Criteria
13	13		Matrix Compression	Post-Failure	Degradation Rule
			Fiber Breakage	DYNA3D	Interactive Criteria

19 ABSTRACT (Continue on reverse if necessary and identify by block number)

A laminated shell formulation and damage model for fiber-composite materials are implemented in DYNA3D, a three-dimensional finite element code to analyze the large deflection and materially nonlinear response of structures and solids. The damage model consists of an interactive failure criterion and a post-failure degradation rule. The failure criterion identifies three modes of failure: matrix cracking, matrix compression failure, and fiber breakage. When a failure criterion is met, some of all or the lamina's elastic constants are set to zero.

The failure model and post-failure degradation rule are compared with experimental results available from the literature to establish the validity of the damage model. Comparisons between the failure criteria and experimental results indicate that the Chang fiber breakage criterion is in agreement with biaxial stress test data if reasonable assumptions are made regarding matrix cracking prior to fiber breakage. However, the matrix failure criteria do not adequately model matrix strength under combined loading conditions. A

20 DISTRIBUTION/AVAILABILITY OF ABSTRACT	21 ABSTRACT SECURITY CLASSIFICATION
☐ UNCLASSIFIED/UNLIMITED ☒ SAME AS REPORT ☐ DTIC USERS	UNCLASSIFIED
22a NAME OF RESPONSIBLE INDIVIDUAL Bennie F. Maddox	22b TELEPHONE (Include Area Code) (703) 325-7042 — 22c OFFICE SYMBOL DNA/CSTI

DD FORM 1473, JUN 86 — Previous editions are obsolete — SECURITY CLASSIFICATION OF THIS PAGE UNCLASSIFIED

19. ABSTRACT (Continued)

modified form of the Tsai-Wu criterion is in better agreement with the test data and is recommended for implementation into DYNA3D. A flexible post-failure degradation rule is also recommended: modifications to the current implementation are suggested which allow the user to specify the degradation behavior for each mode of failure.

SUMMARY

Impulsive loading of structures composed of fiber-composite materials has application in many applied fields. Tests on fiber-composite motor case models indicate a wide range of material damage, including matrix cracking, delamination, and fiber breakage resulting in catastrophic failure of the case. A composite damage model was recently implemented into the nonlinear finite element code DYNA3D (Reference [1]) to analyze impulsively loaded materials and structures. The validity of the composite damage model is assessed in the present report by comparing the model with experimental results.

This summary and the main body of the report are in two sections. The first section is a review of commonly used failure criteria and the development of the Chang interactive criterion currently implemented in DYNA3D. The second section compares failure criteria and post-failure degradation rules with experimental results to assess the validity of the DYNA3D composite damage model. Modifications to both the failure criteria and degradation rules are recommended.

Review and Development of Failure Criteria.

Failure criteria are used to relate critical combinations of stress or strain to failure in a material. Four commonly used failure criteria are the maximum strain, maximum stress, Tsai-Hill, and Tsai-Wu criteria. These criteria are all in agreement for the uniaxial failure stresses in the principal material directions of a lamina. The criteria disagree on what constitutes failure for biaxial stress states.

The maximum stress and maximum strain criteria predict five independent failure modes: tensile and compressive longitudinal failure, tensile and compressive transverse failure, and shear failure. The Tsai-Hill and Tsai-Wu criteria predict only the onset of failure, not the mode of failure, and are called *interactive* criteria because failure depends on more than one stress component.

Hashin in Reference [2] developed a set of interactive failure criteria in which distinct *fiber* and *matrix* failure modes are modeled. Chang in References [3-5] modified Hashin's criteria to include nonlinear shear behavior. Three failure modes are modeled: fiber breakage, matrix cracking, and matrix compression failure. Fiber compressive failure is not modeled. The Chang criteria are implemented in DYNA3D. When failure occurs, some or all of a lamina's elastic constants are set to zero, depending on the mode of failure.

It is important to identify the fiber and matrix failure modes because the effect of each mode on the ultimate strength of a layered composite is quite different. For example, non-catastrophic matrix failure generally precedes catastrophic fiber failure in filament-wound motor cases. Some factors which affect the fiber and matrix failure modes are: properties of the fiber and matrix, fiber volume fraction, and the fiber-matrix bond strength.

Verification of DYNA3D Composite Damage Model.

Calculations were performed to verify the implementation of the failure criteria and degradation rules used in the DYNA3D composite damage model. Each failure mode and degradation rule was demonstrated through calculations on single-element shell laminates. We are satisfied that the failure criteria and degradations rules in our DYNA3D version are implemented correctly.

Computational results are also compared with experimental results found in the literature to establish the validity of the failure criteria and post-failure degradation rules. The Chang failure criteria are compared with three sets of material property tests:

- lamina off-axis tests to verify the tensile failure criteria (fiber and matrix),
- lamina combined stress tests to verify the matrix failure criteria,
- biaxial stress tests on quasi-isotropic laminates to verify the fiber failure criteria.

The Chang fiber breakage criterion is in agreement with biaxial stress test data if reasonable assumptions are made regarding matrix cracking prior to fiber breakage. However, the comparison's indicate that the Chang matrix failure criteria do not adequately model matrix strength under combined loading conditions. A modified form of the Tsai-Wu criterion is in better agreement with the test data and is therefore recommended for implementation into DYNA3D.

Most analytical and experimental results available from the literature determine the post-failure stress-strain response of laminates with cracked plies. One common method for estimating stiffness reductions in laminates with cracked plies is the *ply discount method.* With this method, one or more of the elastic constants of a cracked ply are set equal to zero. A ply discount scheme is currently implemented in DYNA3D.

Tests and analyses results indicate that the reduction in ply properties due to matrix cracking depends on the ply stacking sequence, ply stiffnesses, and cracking ply thickness. The ply discount scheme does not adequately predict the reduction in stiffness. Thus, a general post-failure degradation rule should be implemented into DYNA3D that is capable of modeling ply stiffness reductions for arbitrarily stacked laminates. A flexible post-failure degradation rule is recommended and modifications to the current implementation are suggested which allow the user to specify the degradation behavior for each mode of failure.

PREFACE

This topical report is part of an effort to develop and verify numerical techniques for modeling fiber-composite materials. Numerical results are compared with experimental results available from the literature to test the validity the fiber-composite failure criteria and post-failure degradation rules implemented in DYNA3D. Numerical results which verify the constitutive behavior of the laminated shell model were included in a previous report, *Fibrous Composite Laminates: An Introduction to the Theory, and Verification of the DYNA3D Implementation*, DNA-TR-88-191.

The DNA technical monitors were Dr. Michael Frankel and Maj. Paul J. Wolf. The APTEK program manager was Mr. Stephen H. Sutherland. Suggestions and comments on the topical report were provided by Drs. Leonard E. Schwer and Herbert E. Lindberg of APTEK.

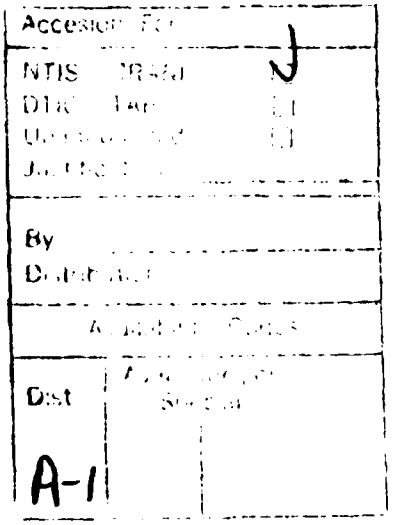

CONVERSION TABLE

Conversion factors for U.S. Customary to metric (SI) units of measurement

MULTIPLY TO GET	BY	TO GET DIVIDE
angstrom	1.000 000 X E -10	meters (m)
atmosphere (normal)	1.013 25 X E +2	kilo pascal (kPa)
bar	1.000 000 X E +2	kilo pascal (kPa)
barn	1.000 000 X E -28	meter^2 (m^2)
British thermal unit (thermochemical)	1.054 350 X E +3	joule (J)
calorie (thermochemical)	4.184 000	joule (J)
cal (thermochemical)/cm^2	4.184 000 X E -2	mega joule/m^2 (MJ/m^2)
curie	3.700 000 X E +1	*giga becquerel (GBq)
degree (angle)	1.745 329 X E -2	radian (rad)
degree Fahrenheit	t_k = (t°f + 459.67)/1.8	degree kelvin (K)
electron volt	1.602 19 X E -19	joule (J)
erg	1.000 000 X E -7	joule (J)
erg/second	1.000 000 X E -7	watt (W)
foot	3.048 000 X E -1	meter (m)
foot-pound-force	1.355 818	joule (J)
gallon (U.S. liquid)	3 785 412 X E -3	meter^3 (m^3)
inch	2.540 000 X E -2	meter (m)
jerk	1.000 000 X E +9	joule (J)
joule/kilogram (J/kg) (radiation dose absorbed)	1.000 000	Gray (Gy)
kilotons	4.183	terajoules
kip (1000 lbf)	4.448 222 X E +3	newton (N)
kip/inch^2 (ksi)	6 894 757 X E +3	kilo pascal (kPa)
ktap	1.000 000 X E +2	newton-second/m^2 ($N-s/m^2$)
micron	1 000 000 X E -6	meter (m)
mil	2.540 000 X E -5	meter (m)
mile (international)	1.609 344 X E +3	meter (m)
ounce	2.834 952 X E -2	kilogram (kg)
pound-force (lbs avoirdupois)	4.448 222	newton (N)
pound-force inch	1.129 848 X E -1	newton-meter (N·m)
pound-force/inch	1 751 268 X E +2	newton/meter (N/m)
pound-force/foot^2	4.788 026 X E -2	kilo pascal (kPa)
pound-force/inch^2 (psi)	6.894 757	kilo pascal (kPa)
pound-mass (lbm avoirdupois)	4.535 924 X E -1	kilogram (kg)
pound-mass-foot^2 (moment of inertia)	4.214 011 X E -2	kilogram-meter^2 ($kg \cdot m^2$)
pound-mass/foot^3	1.601 846 X E +1	kilogram/meter^3 (kg/m^3)
rad (radiation dose absorbed)	1.000 000 X E -2	**Gray (Gy)
roentgen	2.579 760 X E -4	coulomb/kilogram (C/kg)
shake	1.000 000 X E -8	second (s)
slug	1.459 390 X E +1	kilogram (kg)
torr (mm Hg, 0° C)	1.333 22 X E -1	kilo pascal (kPa)

*The becquerel (Bq) is the SI unit of radioactivity; 1 Bq = 1 event/s.
**The Gray (Gy) is the SI unit of absorbed radiation.

TABLE OF CONTENTS

(CONTINUED)

LIST OF ILLUSTRATIONS

LIST OF ILLUSTRATIONS (Continued)

LIST OF TABLES

SECTION 1
BRIEF BACKGROUND ON THE DEVELOPMENT OF COMPOSITE DAMAGE MODELS.

Failure criteria relate critical combinations of stresses or strains to failure in a material. Some criteria predict only the onset of failure, while more sophisticated criteria predict the mode of failure as well. We begin this section by reviewing some of the failure modes observed in fiber-composite materials. The subsection on failure modes is followed by a review of failure criteria that are commonly used by analysts today. Finally, the development of the Chang composite damage model, which is currently implemented in DYNA3D, is presented.

1.1 FAILURE MODES IN UNIDIRECTIONAL COMPOSITES.

Distinct *fiber* and *matrix* failure modes are observed in fiber-composites. It is important to distinguish the modes of failure because the effect of each mode on the ultimate strength of a layered composite is quite different. For example, non-catastrophic matrix cracking generally preceeds fiber breakage (catastrophic) in filament-wound motor cases. Matrix cracking of at-angle plies leads to load redistribution between the hoop and at-angle layers, while fiber breakage often leads to catastrophic failure of the motor case. The factors affecting the fiber and matrix failure modes are briefly discussed in this subsection. Most of this information was obtained from the lecture notes of a UCLA short course on advanced analysis of composite materials, Reference [6]. The course notes on failure modes were presented by Mr. Longin Greszczuk of McDonnell Douglas Space Systems Company (MDSSC).

1.1.1 Fiber Tensile Failure.

Some factors which affect tensile failure in the longitudinal-fiber direction are:

- properties of the fiber and matrix,
- fiber volume fraction,
- fiber-matrix bond strength,
- fiber length,
- nonuniformities (scatter) in fiber strength, modulus, or pre-tension.

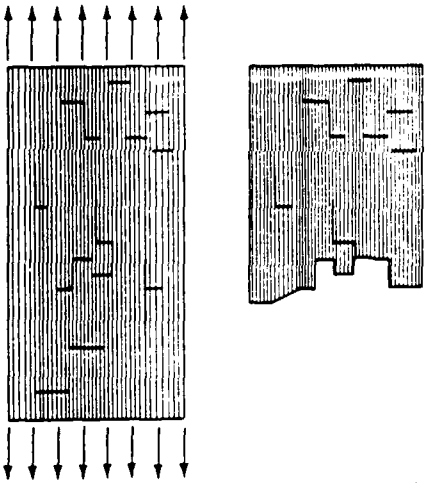

Figure 1. Tensile failure mode in longitudinal fiber-direction.

Fiber misalignment and test methods can also affect the measured strength. For example, a graphite-epoxy specimen tested with fibers oriented at 4° to the test axis exhibits a drop in measured strength of about 17%. This is because the biaxial stress field, in the principal material directions of the composite, causes fiber-matrix debonding or matrix cracking failure at the low transverse tensile and shear strengths of the material. Matrix failure reduces the ability of the composite to carry additional load in the longitudinal-fiber direction. The ability of the matrix to transfer load by shear to an unbroken section of fiber is demonstrated by comparing the ultimate strength of fiber bundles tested with and without a matrix. Greszczuk in Reference [6] reports that the ultimate strength of fiber bundles tested without a matrix material is up to 40% less than that of a fiber-matrix composite.

Tensile tests in the fiber direction of unidirectional polymer-matrix specimens indicate that the failure surface is jagged, as discussed in References [7] and [8]. Random fiber breaks lead to matrix cracks both transverse to the fibers and along the fiber direction, as shown schematically in Figure 1. Transverse cracks coalesce, reducing the load carrying capacity of the specimen, until complete fiber breakage failure occurs.

Longitudinal tensile strength is commonly modeled with either a rule of mixtures or a statistical flaw model. The rule of mixtures relates the longitudinal tensile strength of the composite to the strength of the fiber and matrix components in proportion to the volume fraction of each component. The rule of mixtures tends to overestimate the strength of composites with poor fiber-matrix interfaces. The flaw model considers the statistical nature of fiber breakage by including a constant which is a measure of scatter in fiber strength. Fiber length is included in determining the scatter because longer fibers have more flaws, hence break at lower failure stresses

than shorter fibers. An ineffective fiber length is also included in the model. When a fiber breaks, the load is transferred by shear in the matrix back to the fiber a short distance along its length from the break. The ineffective fiber length is that length required to pick up a certain percentage of the load, and is thus a measure of the load redistribution capability of the composite. Further discussion of the statistical flaw model is given in References [8-9] by Rosen.

1.1.2 Fiber Compressive Failure.

Compressive failure in the longitudinal-fiber direction is strongly influenced by the following factors:

- fiber and matrix properties,
- fiber-matrix bond strength,
- the fiber volume fraction.

Possible failure modes include microbuckling of bonded or debonded fibers, interaction failure, or direct fiber failure. These failure modes are reported by Greszczuk in Reference [10] and discussed in the following paragraphs.

Microbuckling with Bonded Fibers. For fibers well bonded to the matrix, this type of microstructural failure can occur under compression in either the extensional mode or shear mode, as shown in Figure 2 and discussed in References [11] and [12]. In the extensional mode, the matrix extends or contracts in the direction perpendicular to the fibers. In the shear mode, the matrix deforms primarily in a shear deformation between adjacent fibers. The mode depends on the fiber volume fraction, and moduli of the fibers and matrix. The most common mode for practical fiber composites is the shear mode. Microbuckling doesn't necessarily damage the fibers unless it is followed by kinking of the fibers. A schematic of fiber kinking and subsequent fracture is shown in Figure 3. Kink band formation has been observed in Kevlar, glass, and graphite composites, as discussed in References [12-13].

Microbuckling with Unbonded Fibers. A failure mode for composites with a weak fiber-matrix interface is fiber-matrix debonding followed by microbuckling in the shear mode. Microbuckling theory, and tests conducted by Greszczuk on ideal composites (metal rods in a matrix) indicate that the strength of composites with unbonded fibers is substantially less than that with bonded fibers. Hahn *et al.* in Reference [12] also observed that microbuckling is initiated at regions of local inhomogenities, such as voids, stress concentrations, or weak matrix areas. Microbuckling of unbonded fibers can also be followed by fiber kinking.

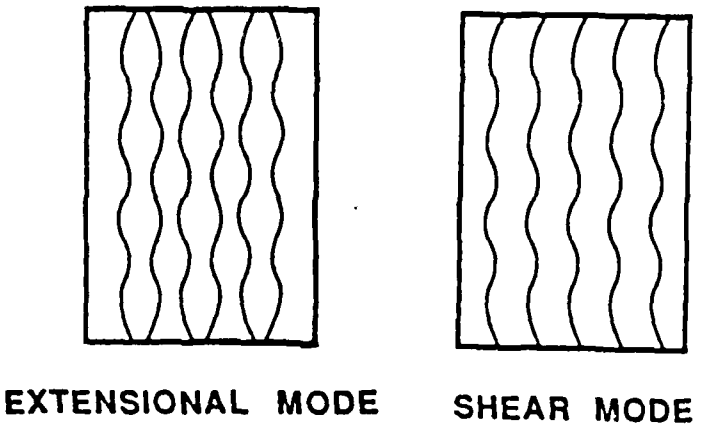

Figure 2. Microbuckling failure modes.

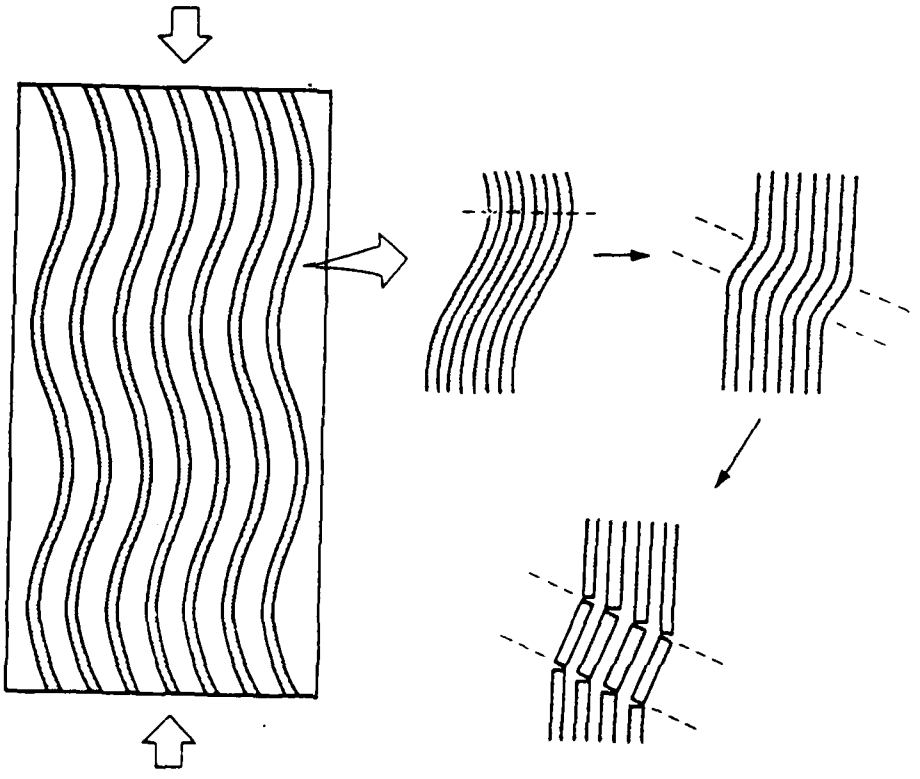

Figure 3. Kink band formation and fracture following microbuckling.

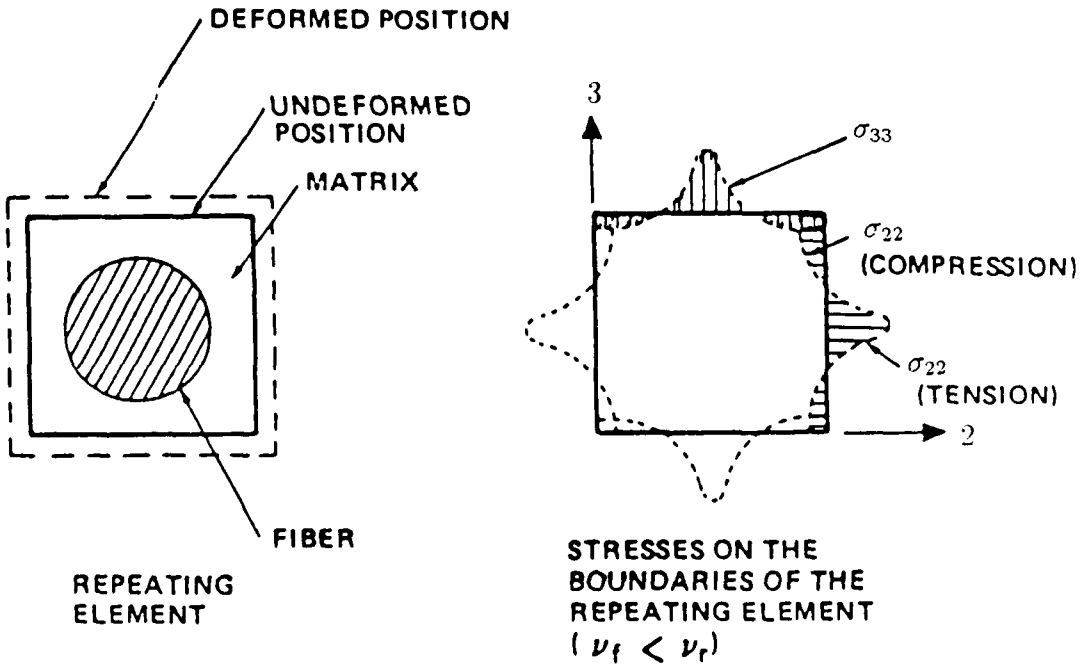

Figure 4. Interaction failure mechanism in fiber composites.

Interaction Failure. When a unidirectional composite is loaded in longitudinal compression, transverse tensile and compressive stresses develop in the matrix because of the differences in Poisson's ratios between the fibers and the matrix, as shown in Figure 4. Consider a compressive load applied to unidirectional composite in the fiber direction. Stresses develop in the matrix in the transverse-fiber directions. The distribution of stress in the matrix adjacent to a single fiber, called a *repeating element*, is shown in Figure 4 for the case when Poisson's ratio of the fiber, ν_f, is less than Poisson's ratio of the matrix, ν_r. If the matrix transverse tensile strength is low, matrix cracking, fiber-matrix debonding, or delaminations may occur. As an example, test data are compared in Figure 5 with a theory developed by Greszczuk and Pagano. The theory relates the ratio of the ultimate compression strength with interaction, F_{Lc}, and compression strength without interaction, $F_f k_f$ (F_f is the fiber compressive strength and k_f is the fiber volume fraction), to the transverse tensile strength, F_{Tt}.

Direct Fiber Failure. Fiber compression failure occurs before microbuckling if the fibers are weak in compression.

A comparison of test data with calculated stresses for each of the compressive failure modes just discussed is shown in Table 1. This table is reproduced from Reference [6]. Note that the measured failure strength of Kevlar-epoxy is close to that calculated from microbuckling theory for unbonded fibers. Fiber kinking following microbuckling is also reported for Kevlar-epoxy in Reference [13]. A flow chart

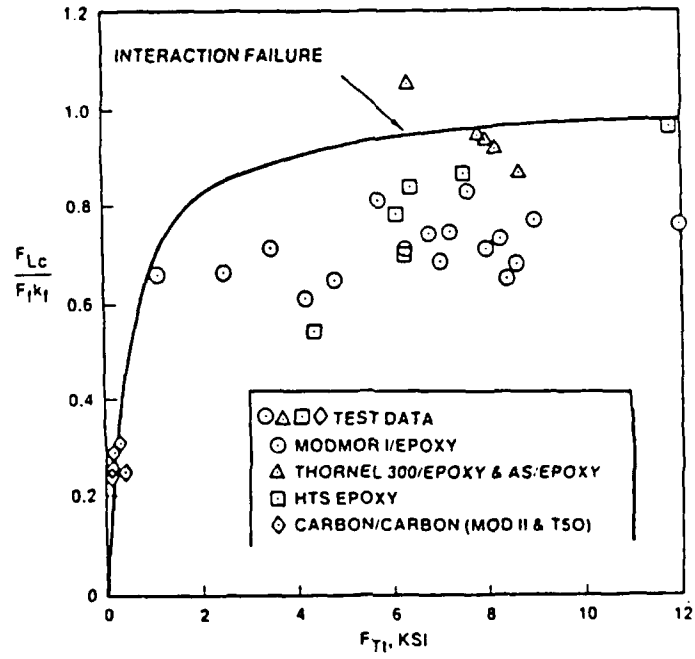

Figure 5. Comparison of interaction failure theory with test data.

(reproduced from Reference [12]) which describes the microstructural compression response of fiber composites is shown in Figure 6. The failure sequence suggested for unidirectional graphite and glass reinforced composites is given by the shaded boxes. The chart suggests that microbuckling, followed by fiber kinking or bending failure due to continued microbuckling, are the dominate compressive failure modes for these composites.

1.1.3 Matrix Failure due to Transverse Fiber Stress and Shear Stress.

The primary factors affecting the transverse tensile, compressive, and shear strengths of a composite are:

- properties of the fiber and matrix (such as transverse Young's moduli for transverse failure and shear moduli for shear failure),
- fiber volume fraction,
- void content,
- fiber-matrix bond strength,
- stress concentrations from bonded fibers and from voids.

Table 1. Comparison of compressive stresses from four theoretical failure modes with data from composites made with rigid resins.

Measured Data *vs.* Theoretical Modes	Composites			
	Unbonded Steel Rods in Epoxy (MPa)	Bonded Steel Rods in Epoxy (MPa)	Modmor II Epoxy (MPa)	Kevlar Epoxy (MPa)
Measured Data:	481	887	972	276
Theoretical Failure Modes:				
Microbuckling (Bonded Fibers)	—	6255	4552	2069
Microbuckling (Unbonded Fibers)	533	—	372	372
Interaction Failure	—	881	1200	1207
Direct Fiber Failure	—	946	1338	1517

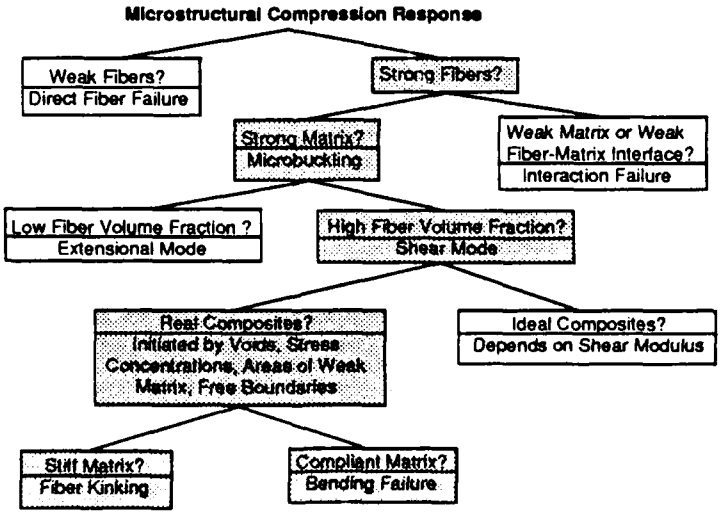

Figure 6. Micromechanical compression failure modes of fiber composites. The shaded boxes give the failure sequence suggested for unidirectional graphite and glass reinforced composites.

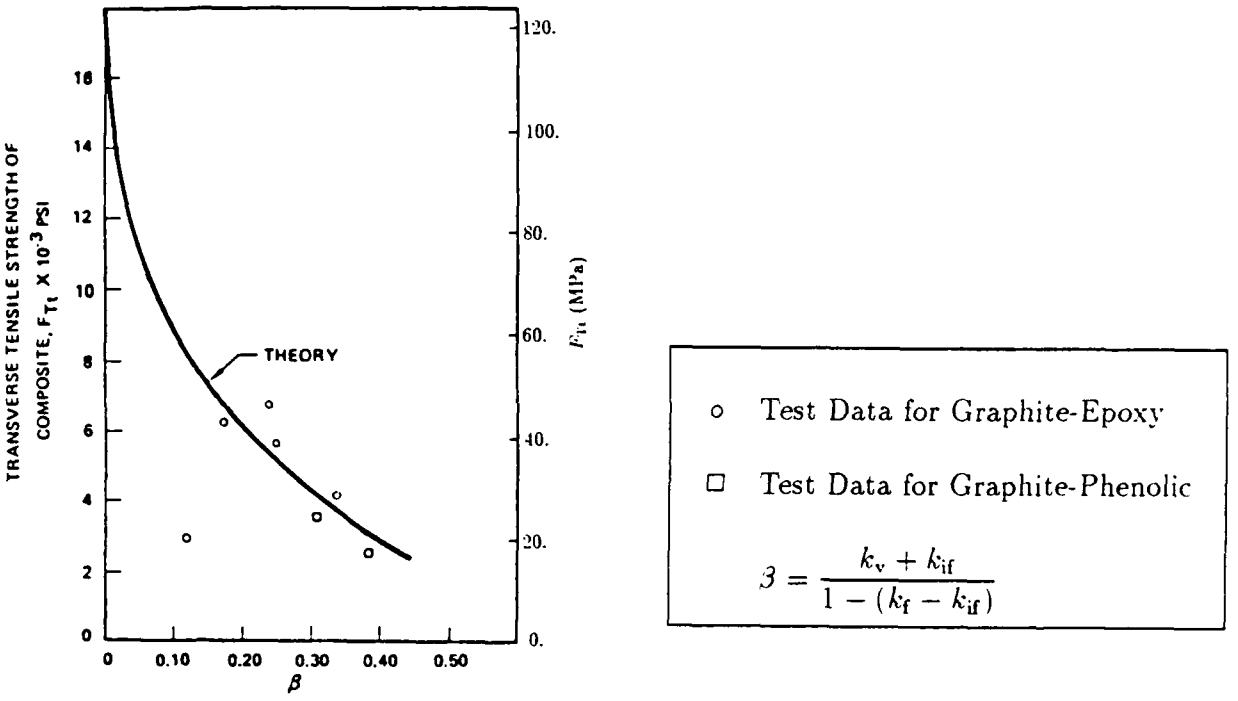

Figure 7. Comparison of test data with theory for transverse tensile failure of graphite-epoxy.

Greszczuk in Reference [6] shows that the interaction of triaxial stress concentrations from fibers and voids, and the number of unbonded or ineffective fibers aligned at the boundary of voids, have a strong effect on transverse tensile strength. As an example, the transverse tensile strengths of composites made with graphite fibers and different resins are compared in Figure 7 with a theory developed by Greszczuk. The abscissa parameter, β, depends on the volume fractions of fibers (k_f), voids (k_v), and ineffective fibers (k_{if}). Good agreement between test data and theory is also reported by Greszczuk for S-glass fibers embedded in different resins (not shown). For S-glass composites, Greszczuk shows that the transverse tensile strength approaches (and exceeds slightly) the tensile strength of the resin as $\beta \rightarrow 0$, *i.e.* as the void and ineffective-fiber fractions approach zero.

Tensile tests in the transverse fiber direction of unidirectional specimens indicate that cracks form in the matrix parallel to the fiber direction, as discussed in Reference [8] and shown schematically in Figure 8. Both transverse fiber and shear stresses are assumed to contribute to the tensile matrix failure mode. For transverse fiber compressive stress, matrix compression failure occurs. Compression failure occurs by shearing in the matrix in a plane parallel to the fibers, but not necessarily normal to the direction of the applied compressive stress. A schematic of matrix compression failure is shown in Figure 9. Both transverse fiber compressive stress and shear stress are assumed to contribute to the matrix compressive failure mode.

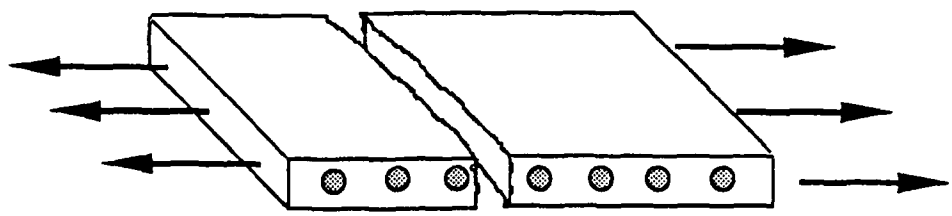

Figure 8. Matrix tensile failure mode in unidirectional composite.

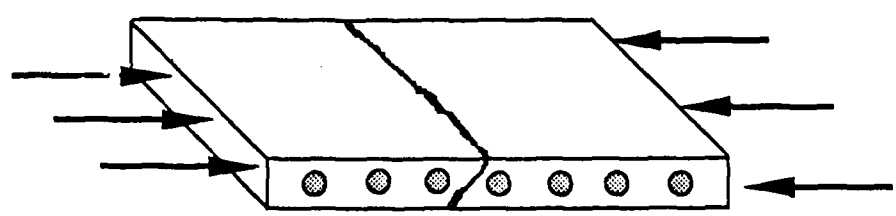

Figure 9. Matrix compression failure mode in unidirectional composite.

1.1.4 Comments on Strength Coupling.

As discussed in the preceeding sections, both tensile and compressive fiber failure strengths are coupled with the matrix and fiber-matrix debond strengths. Matrix failure reduces the ability of the matrix to transfer load through the lamina, which reduces the fiber tensile failure strength of the composite. Fiber composites can also fail in longitudinal compression due to low matrix strength. Strength coupling is also path dependent. For example, Wu in Reference [6] suggests that broken fibers can initiate transverse matrix cracks, thus reducing the transverse tensile strength of the composite. Biaxial stress tests should be performed on unidirectional composites to aid in understanding strength coupling and to validate interactive failure criteria.

1.2 REVIEW OF FAILURE CRITERIA.

Failure criteria are used to relate critical combinations of stresses or strains to failure in a material. Numerous failure criteria are available to predict the strength of laminated materials, References [14-20]. Simple criteria are applied directly to the total laminate, but more complete criteria are applied to the individual layers of the laminate.

In direct laminate failure criteria, the laminate is considered to be homogeneous and anisotropic. Lamination theory is not required to analyze the stresses and strains in each layer. However, the criteria are difficult to use because laminate strengths must be determined for each layup that is analyzed.

Lamina-by-lamina failure criteria are more common than laminate failure criteria because they are more general, and hence more universally applicable. Only one set of material property tests need be performed on unidirectional specimens to determine the strength characteristics of the fiber composite lamina, and then any layup can be analyzed. Lamination theory is used to obtain the stresses and strains in the principal material directions of each lamina. The failure criteria are applied to each lamina to predict lamina-by-lamina failure.

Lamina failure criteria are macromechanical because the average stress and strain in the lamina are used to predict failure. The lamina are considered to be homogeneous and orthotropic. Micromechanical failure criteria are less common than macromechanical failure criteria because of the complexity of dealing with the interaction of the fiber and matrix components. However, guidelines based on micromechanics, such as understanding how the stresses in the fiber, matrix, and fiber-matrix interface each contribute to failure, are used to establish failure criteria that distinguish between failure modes.

Sometimes micromechanics is used to predict the strength of the lamina from the strength of the components, but more often, lamina strengths are obtained experimentally from uniaxial tests on unidirectional specimens. A few criteria also require biaxial test data. The strengths measured for use in a plane-stress failure criteria

are generally the tensile and compressive strengths in the fiber direction, the tensile and compressive strengths in the transverse fiber direction, and the in-plane shear strength. Failure modes of unidirectional fiber-composites are discussed in Section 1.2.

The failure surface of an orthotropic lamina in a state of plane stress is three-dimensional. It is defined in stress space by the stresses in the principal material directions of the lamina, σ_{11}, σ_{22}, and σ_{12} (σ_1, σ_2, and σ_6 in contracted notation). The intercepts of the failure surface with the coordinate axes are the material strengths measured from uniaxial tests on unidirectional specimens. For simplicity, the failure envelope can be plotted as a curve in σ_{11} , σ_{22} stress space, for constant values of σ_{12}. Most criteria are in agreement for the failure stresses in the principal material directions, *i.e.* the intercepts of the failure surfaces with the coordinate axes are in agreement. The criteria differ on what constitutes failure for biaxial stress states.

A survey of the most commonly used failure criteria was conducted by the American Institute of Aeronautics and Astronautics (AIAA) to determine how much variability exists in the design and analysis of composite structures, Reference [14]. The survey results indicate that the maximum stress, maximum strain, Tsai-Hill, and Tsai-Wu failure criteria are most often used by surveyed AIAA members. These failure criteria are discussed in the following paragraphs.

Maximum Stress. Failure occurs when any component of stress in the principal material directions of the lamina exceeds its corresponding strength:

$$\begin{array}{rcll} \sigma_{11} & \geq & X_T & (\sigma_{11} > 0) \\ |\sigma_{11}| & \geq & X_C & (\sigma_{11} < 0) \\ \sigma_{22} & \geq & Y_T & (\sigma_{22} > 0) \\ |\sigma_{22}| & \geq & Y_C & (\sigma_{22} < 0) \\ |\sigma_{12}| & \geq & S & \end{array}$$

The five ultimate strengths are determined from uniaxial and pure-shear tests on unidirectional specimens:

X_T	Tensile strength in longitudinal fiber direction
X_C	Compressive strength in longitudinal fiber direction
Y_T	Tensile strength in transverse fiber direction
Y_C	Compressive strength in transverse fiber direction
S	In-plane shear strength

Five independent modes of failure are predicted: tensile and compressive longitudinal failure, tensile and compressive transverse failure, and shear failure.

Maximum Strain. Failure occurs when any strain component in the principal material directions of the lamina exceeds its corresponding ultimate strain. Five ultimate

strain values are determined from uniaxial and pure shear tests on unidirectional specimens; the ultimate tensile and compressive strains in the fiber and transverse fiber directions, and the ultimate shear strain. Five failure modes are also predicted: tensile and compressive failure in the longitudinal fiber and transverse fiber directions, and shear failure. These are the same failure modes predicted with the maximum stress criteria. The maximum strain failure criteria allow for some interaction among the in-plane stresses through the Poisson effect.

Tsai-Hill. This failure criterion is a generalization of the maximum distortional energy criterion for isotropic materials. Hill, in Reference [15], extended the criterion to orthotropic materials. Tsai and Azzi, in Reference [16], modified the Hill criterion to account for the plane stress conditions and transverse isotropy of fiber composite lamina:

$$\frac{\sigma_{11}^2}{X^2} - \frac{\sigma_{11}\sigma_{22}}{X^2} + \frac{\sigma_{22}^2}{Y^2} + \frac{\sigma_{12}^2}{S^2} \geq 1 \tag{1}$$

where X and Y are the in-plane strengths in the fiber and transverse fiber directions, respectively, and S is the in-plane shear strength. Tsai showed that the criterion is applicable to composites with different properties in tension and compression. Tensile strengths are used when the corresponding stresses are tensile, and compressive strengths are used when the corresponding stresses are compressive. Tsai also developed two additional equations for mutually orthogonal planes, similar to Equation (1), for failure analysis of three-dimensional materials, Reference [17].

The Tsai-Hill criterion is called an *interactive failure criteria* because failure depends on more than one value of stress. The failure surface for the Tsai-Hill criterion is a smooth surface (ellipsoidal or spherical, depending on the strength values) in σ_{11}, σ_{22}, σ_{12} stress space. In contrast, the failure surfaces of the maximum stress and maximum strain criteria are not smooth surfaces because they are formed by intersecting planes. Unlike the maximum stress and strain criteria, the mode of failure is not predicted by the Tsai-Hill criterion. These two types of criteria are analogous to Tresca-type (intersecting planes) and Mises-type (smooth surface) criteria for homogeneous isotropic materials.

Tsai-Wu. Tsai and Wu developed a tensor-component polynomial theory as a failure criterion for anisotropic materials, Reference [18]. The criterion contains linear as well as quadratic stress terms. Failure occurs when the following equation is satisfied:

$$F_1\sigma_{11} + F_2\sigma_{22} + F_{11}\sigma_{11}^2 + F_{22}^2\sigma_{22}^2 + F_{12}\sigma_{11}\sigma_{22} + F_{66}\sigma_{12}^2 \geq 1 \tag{2}$$

Six coefficients must be defined for a composite lamina in a state of plane stress. Five coefficients ($F_1, F_2, F_{11}, F_{22}, F_{66}$) are determined from uniaxial and shear tests on unidirectional specimens. Each of the coefficients, F_1, F_2, F_{11}, and F_{22} include contributions from both tensile and compressive strengths (see, for example, Equation 26), rather than requiring separate values for tension and compression as for the X and Y strengths in the Tsai-Hill criterion. The sixth coefficient, F_{12}, must be determined from biaxial tests, a variety of which are available. Unfortunately, different

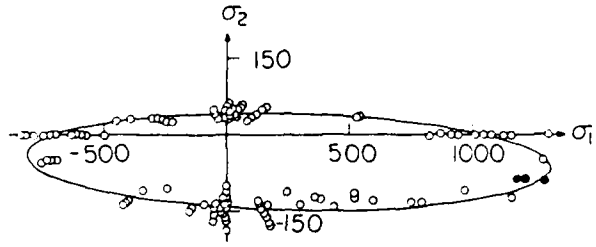

(a) Tsai-Wu Polynomial RMS=0.137

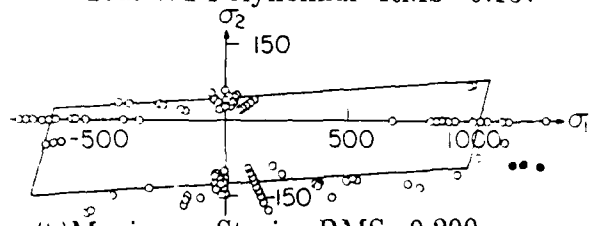

(b) Maximum Strain RMS=0.200

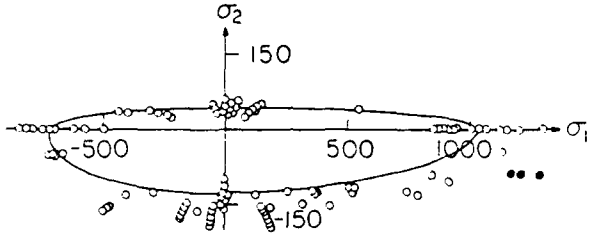

(c) Tsai-Hill RMS=0.226

Figure 10. Comparison of three commonly used failure criteria with graphite-epoxy test data.

tests produce different values of F_{12}. Like the Tsai-Hill failure criterion, the failure envelope is a smooth surface in stress space and only the onset of failure is predicted, not the mode of failure.

The AIAA survey indicated that the maximum strain criterion is the most frequently used failure criterion, followed by the maximum stress, Tsai-Hill, and Tsai-Wu criteria. The ability of each criterion to predict experimental data varies from one composite material to another. Comparison of three of the failure criteria with test data for graphite-epoxy is shown in Figure 10. This figure is reproduced from Reference [19]. The root mean square (RMS) values indicate how well the criteria fit the test data. An advantage of the maximum strain and maximum stress criteria is that the mode of failure is predicted. With the mode of failure identified, progressive damage in the laminate can be analyzed by including degradation of lamina properties.

The Chang criteria, which are currently implemented in DYNA3D, are not compared with test data in Figure 10, because material strengths and failure modes were not reported for the test data. The Chang criteria are discussed in detail in Section 1.3.

1.3 DEVELOPMENT OF CHANG'S FAILURE CRITERIA.

As discussed in Section 1.1, the Tsai-Hill and Tsai-Wu interactive failure criteria predict when a given set of stresses and strains will produce failure, but they do not give the mode of failure. Hashin developed an interactive failure criterion, Reference [2], in which four distinct failure modes are modeled: tensile and compressive fiber failure and tensile and compressive matrix failure. Chang modified Hashin's criterion to include nonlinear shear stress-strain behavior. Chang also defined a post-failure degradation rule so that the behavior of the laminate can be analyzed after each sucessive lamina fails. The Chang failure criterion, References [3-5] is used in the DYNA3D composite damage model. In the following discussion, Hashin's failure criterion, and then Chang's modification to include nonlinear shear behavior, are presented. Finally, the DYNA3D post-failure degradation rule is summarized.

1.3.1 Hashin Failure Criteria.

Hashin's three-dimensional failure criteria were established for unidirectional fiber composites in terms of a quadratic stress polynomial. Since most fiber composites are transversely isotropic, Hashin first defined a general failure criterion in terms of the stress invariants of a transversely isotropic material. The three-dimensional criterion has the general form:

$$A_1 I_1 + B_1 I_1^2 + A_2 I_2 + B_2 I_2^2 + C_{12} I_1 I_2 + A_3 I_3 + A_4 I_4 \geq 1 \tag{3}$$

where I_1, I_2, I_3, and I_4 are the stress invariants;

$$\begin{aligned} I_1 &= \sigma_{11} \\ I_2 &= \sigma_{22} + \sigma_{33} \\ I_3 &= \sigma_{23}^2 - \sigma_{22}\sigma_{33} \\ I_4 &= \sigma_{12}^2 + \sigma_{13}^2 \end{aligned} \tag{4}$$

Hashin simplified the criterion for fiber composites in a state of plane stress. Hashin argued that failure is produced by the normal and shear stresses acting on the failure plane. For *fiber* failure, the failure plane is the 2-3 plane, acted on by stresses σ_{11} and σ_{12}. The stress in the transverse fiber direction (σ_{22}) does not contribute to fiber failure. In *matrix* failure, a plane crack occurs parallel to the fiber direction. Failure occurs in any plane with axes parallel and transverse to the fibers. The matrix failure plane is acted on by stresses σ_{22} and σ_{12}. He argued that the stress in the longitudinal fiber direction (σ_{11}) does not contribute to matrix failure because this stress is carried almost entirely by the fibers.

Hashin's plane stress failure criteria, defined in terms of the five principal strengths of a fiber composite, are:

Fiber Tensile Failure: Hashin assumed that tensile and shear stresses are mutually weakening, hence both contribute to fiber breakage. This criterion is also known as the Yamada-Sun failure criterion, Reference [21]. The Yamada-Sun failure criterion is a simplified form of the Tsai-Hill criterion, Equation 1, expressed with the transverse fiber stress set equal to zero ($\sigma_{22} = 0$).

$$\left(\frac{\sigma_{11}}{X_T}\right)^2 + \left(\frac{\sigma_{12}}{S}\right)^2 \geq 1 \qquad (\sigma_{11} > 0) \tag{5}$$

Fiber Compressive Failure: Hashin represents fiber compressive failure in simple maximum stress form. Hashin argued that there is no physically reasonable method for including the effect of shear stress.

$$\sigma_{11} \geq X_C \qquad (\sigma_{11} < 0) \tag{6}$$

Matrix Tensile Failure: Hashin's matrix tensile failure criterion is a simplified form of the Tsai-Hill criterion, Equation 1, expressed with the longitudinal fiber stress set equal to zero ($\sigma_{11} = 0$).

$$\left(\frac{\sigma_{22}}{Y_T}\right)^2 + \left(\frac{\sigma_{12}}{S}\right)^2 \geq 1 \qquad (\sigma_{22} > 0) \tag{7}$$

Matrix Compressive Failure: Matrix failure in the transverse fiber direction depends on the compressive strength in the transverse fiber direction, Y_C, the in-plane shear strength, S, and the transverse shear strength, S_T. Hashin's matrix compression failure criterion contains a first-order term in σ_{22} whose sign depends on Y_C and S_T. The effect of this linear term on the lamina failure envelope is discussed in Section 2.2.

$$\left(\frac{\sigma_{22}}{2S_T}\right)^2 + \left[\left(\frac{Y_C}{2S_T}\right)^2 - 1\right]\frac{\sigma_{22}}{Y_C} + \left(\frac{\sigma_{12}}{S}\right)^2 \geq 1 \qquad (\sigma_{22} < 0) \tag{8}$$

1.3.2 Chang Failure Criteria used in DYNA3D Composite Damage Model.

Chang *et al.*, References [3-5], used a modified form of Hashin's fiber breakage, matrix tensile, and matrix compressive failure criteria to analyze the failure strength of laminates exhibiting nonlinear shear behavior. Chang modified each of the failure criteria to include nonlinear shear effects, following Sandhu's strain energy method, Reference [22]. The modified form of the fiber breakage failure criterion (Equation 5) is:

$$\left(\frac{\sigma_{11}}{X_T}\right)^2 + \frac{\int_0^{\gamma_{12}} \sigma_{12} d\gamma_{12}}{\int_0^{\gamma_{12}^u} \sigma_{12} d\gamma_{12}} \geq 1 \tag{9}$$

where γ_{12}^u is the ultimate shear strain of the lamina. Chang used the nonlinear shear stress-strain relation advanced by Hahn and Tsai, Reference [23], in Equation 9:

$$\gamma_{12} = \frac{1}{G_{12}}\sigma_{12} + \alpha\sigma_{12}^3 \tag{10}$$

where α is the nonlinear shear stress parameter. This parameter is included in the shear stress-strain formula to describe the nonlinear behavior typical of many fiber-composite materials. The parameter α is determined from materials testing. We refer to the term containing the shear stress-strain integrals as the fiber-matrix shearing term. By performing the indicated integration, the fiber-matrix shearing term, $\bar{\tau}$, is defined as follows:

$$\bar{\tau} = \left(\frac{\sigma_{12}}{S}\right)^2 \left\{\frac{1 + \frac{3}{2}\alpha G_{12}\sigma_{12}^2}{1 + \frac{3}{2}\alpha G_{12}S^2}\right\} \tag{11}$$

For $\alpha = 0$, this term reduces to the ratio of the shear stress to shear strength, $(\sigma_{12}/S)^2$, used in the Hashin criteria, Equations 5, 7, and 8. For $\alpha > 0$, the term in brackets is less than one so that $\bar{\tau} < (\sigma_{12}/S)^2$. Hashin's tensile and compressive matrix failure models are also modified in a similar manner to account for nonlinear shearing.

When a failure criterion is met, some or all of the lamina's elastic constants are set to zero, following a method Chang pursued in early unpublished works. These degradation rules were made available to us through personal communication with Dr. Chang. More recently, Chang improved on his post-failure degradation rules and published results in References [3-5]. We will therefore refer to the degradation rules implemented in DYNA3D as the DYNA3D post-failure model.

The DYNA3D post-failure model is an *ad hoc* treatment of post-failure degradation and is characterized as a 'strain softening' constitutive response, *e.g.* after failure the strain continues to increase under constant or decreasing load. One fundamental problem with the implementation of strain softening models into finite element codes is mesh size dependency, *i.e.* the same physical problem will produce different results for different mesh configurations. Strain softening effects in the current composite damage model version of DYNA3D have not been investigated. However, Simo in Reference [24] developed a mathematically rigorous approach to strain softening, which he calls the principal of *Maximum Damage Dissipation.* His work was supported, in part, by a subcontract from APTEK and may be utilized in future efforts.

The complete failure criteria advanced by Chang and DYNA3D post-failure degradation rules are defined in the following paragraphs. In his criteria, Chang suggests using the *in situ* in-plane shear strength measured from tests on symmetric cross-ply laminates, rather than the shear strength measured from tests on unidirectional specimens. Chang and Springer in Reference [4] state that the shear strength of a three-layered glass-epoxy composite is two to three times greater than that obtained by testing single plies.

Fiber Breakage Failure Criterion:

$$\left(\frac{\sigma_{11}}{X_T}\right)^2 + \bar{\tau} \geq \qquad (\sigma_{11} > 0) \tag{12}$$

When the fiber breakage failure criterion is satisfied, all of the elastic constants of the failed lamina are set to zero, *i.e.* $E_{11} = E_{22} = G_{12} = \nu_{12} = \nu_{21} = 0$. The lamina is no longer able to carry load in the fiber, transverse fiber, or shear directions. The load is redistributed to the remaining lamina.

Matrix Cracking Failure Criterion:

$$\left(\frac{\sigma_{22}}{Y_T}\right)^2 + \bar{\tau} \geq 1 \qquad (\sigma_{22} > 0) \tag{13}$$

When the matrix cracking failure criterion is satisfied, all of the elastic constants except for the fiber modulus, E_{11}, are set to zero, *i.e.* $E_{22} = G_{12} = \nu_{12} = \nu_{21} = 0$. The lamina is unable to carry load in the transverse fiber or shear directions. Once matrix cracking failure occurs, both the stress in the transverse fiber direction and shear stress are reduced to zero.

Matrix Compression Failure Criterion:

$$\left(\frac{\sigma_{22}}{2S}\right)^2 + \left[\left(\frac{Y_C}{2S}\right)^2 - 1\right]\frac{\sigma_{22}}{Y_C} + \bar{\tau} \geq 1 \qquad (\sigma_{22} < 0) \tag{14}$$

When the matrix compression failure criterion is satisfied, the transverse elastic modulus and both Poisson's ratios are set to zero, *i.e.* $E_{22} = \nu_{12} = \nu_{21} = 0$. The lamina is unable to carry load in the transverse fiber direction; the stress in the transverse fiber direction is reduced to zero. Note that in Equation 14 Chang has replaced the transverse shear strength, S_T, in Hashin's criterion, Equation 8, with the in-plane shear strength, S.

The above failure criteria and post-failure degradation rules, which we refer to as the Chang failure criteria, are used in the DYNA3D composite damage model. The Chang criteria, along with the other fiber-composite failure criteria[1], are given in Table 2. The Chang criteria do not model all types of damage observed in fiber composite materials, *e.g.* fiber compression failure and delamination. Static fiber-direction compression tests on Kevlar-epoxy indicate that the stress-strain response curves can be modeled as elastic-perfectly plastic, as suggested in References [25] and [26]. The probable failure mode is microbuckling of debonded fibers. A fiber compressive failure model will be implemented in APTEK's version of DYNA3D once an appropriate degradation rule is established. Dr. Hallquist has also implemented into DYNA3D a failure criterion based on a free-edge delamination model for the composite brick elements, but the criterion has not been verified by APTEK.

[1]The modified Tsai-Wu criterion for matrix tensile and compressive failure is discussed in Section 2.3.3.

Table 2. Failure criteria for fiber-composite materials.

Maximum Stress:	
Fiber Tension	$\sigma_{11} \geq X_T \quad (\sigma_{11} > 0)$
Fiber Compression	$\lvert\sigma_{11}\rvert \geq X_C \quad (\sigma_{11} < 0)$
Matrix Tension	$\sigma_{22} \geq Y_T \quad (\sigma_{22} > 0)$
Matrix Compression	$\lvert\sigma_{22}\rvert \geq Y_C \quad (\sigma_{22} < 0)$
Matrix Shear	$\lvert\sigma_{12}\rvert \geq S$
Tsai-Hill	$\frac{\sigma_{11}^2}{X^2} - \frac{\sigma_{11}\sigma_{22}}{X^2} + \frac{\sigma_{22}^2}{Y^2} + \frac{\sigma_{12}^2}{S^2} \geq 1$
Tsai-Wu	$F_1\sigma_{11} + F_2\sigma_{22} + F_{11}\sigma_{11}^2 + F_{22}^2\sigma_{22}^2 + F_{12}\sigma_{11}\sigma_{22} + F_{66}\sigma_{12}^2 \geq 1$ $F_1 = \frac{1}{X_T} - \frac{1}{X_C} \qquad F_2 = \frac{1}{Y_T} - \frac{1}{Y_C}$ $F_{11} = \frac{1}{X_T X_C} \qquad F_{22} = \frac{1}{Y_T Y_C} \qquad F_{66} = \frac{1}{S^2}$
Modified Tsai-Wu:	
Matrix Failure	$F_2\sigma_{22} + F_{22}^2\sigma_{22}^2 + F_{66}\sigma_{12}^2 \geq 1$
Hashin:	
Fiber Tension	$\left(\frac{\sigma_{11}}{X_T}\right)^2 + \left(\frac{\sigma_{12}}{S}\right)^2 \geq 1 \quad (\sigma_{11} > 0)$
Fiber Compression	$\lvert\sigma_{11}\rvert \geq X_C \quad (\sigma_{11} < 0)$
Matrix Tension	$\left(\frac{\sigma_{22}}{Y_T}\right)^2 + \left(\frac{\sigma_{12}}{S}\right)^2 \geq 1 \quad (\sigma_{22} > 0)$
Matrix Compression	$\left(\frac{\sigma_{22}}{2S_T}\right)^2 + \left[\left(\frac{Y_C}{2S_T}\right)^2 - 1\right]\frac{\sigma_{22}}{Y_C} + \left(\frac{\sigma_{12}}{S}\right)^2 \geq 1 \quad (\sigma_{22} < 0)$
Chang:	
Fiber Breakage	$\left(\frac{\sigma_{11}}{X_T}\right)^2 + \bar{\tau} \geq 1 \quad (\sigma_{11} > 0)$
Matrix Cracking	$\left(\frac{\sigma_{22}}{Y_T}\right)^2 + \bar{\tau} \geq 1 \quad (\sigma_{22} > 0)$
Matrix Compression	$\left(\frac{\sigma_{22}}{2S}\right)^2 + \left[\left(\frac{Y_C}{2S}\right)^2 - 1\right]\frac{\sigma_{22}}{Y_C} + \bar{\tau} \geq 1 \quad (\sigma_{22} < 0)$
	$\bar{\tau} = \left(\frac{\sigma_{12}}{S}\right)^2 \left\{\frac{1 + \frac{3}{2}\alpha G_{12}\sigma_{12}^2}{1 + \frac{3}{2}\alpha G_{12} S^2}\right\}$

SECTION 2
VERIFICATION OF DYNA3D COMPOSITE SHELL DAMAGE MODEL.

Calculations were performed to verify the implementation of the failure criteria and degradation rules used in the DYNA3D composite damage model. Each failure mode and degradation rule is demonstrated through calculations on single-element shell laminates. Computational results, using the damage model, are also compared with experimental results found in the literature to verify the theoretical basis of the failure criteria and post-failure degradation rules. Theoretical aspects of the failure criteria were also evaluated by Dr. Juan Simo and Dr. Junho Jang of Stanford University, under subcontract to APTEK. Their efforts are included in two separate reports, References [27] and [24].

2.1 CALCULATIONS TO DEMONSTRATE FAILURE MODES.

The Chang composite damage model in DYNA3D treats three modes of damage: fiber breakage (tensile failure), matrix cracking (tensile failure), and matrix compression failure. Four material strength parameters are used in the three failure criteria: longitudinal tensile strength X_T, transverse tensile strength Y_T, transverse compressive strength Y_C, and shear strength S. A fifth parameter, the nonlinear shear stress parameter, α, is also included in the damage model to describe the nonlinear in-plane shear stress-strain behavior. For each damage mode, failure in a lamina occurs when a combination of the stresses exceeds the appropriate strength relation for the material. A mathematical description of the damage model was included in Section 1.3.

Calculations were performed to verify the implementation of the fiber and matrix failure modes in DYNA3D. Velocities were applied to each node of an element composed of a single orthotropic lamina to achieve a state of combined extensional and shear strain. The strains in the element increased steadily until failure occured. The material strength parameters were selected so that lamina failure in each of the damage modes would occur at a specified strain level, corresponding to a known stress level. The purpose of these calculations was to verify the implementation for each of the three failure criteria by comparing the stress level at failure with the computed failure stress; we are satisfied that the failure criteria in our DYNA3D version are implemented correctly. Elastic constants and strengths used in the verification calculations are listed in Table 3.

Table 3. Material properties used in verification calculations.

E_{11}	=	51,710	MPa	(7500 ksi)
E_{22}	=	6,897	MPa	(1000 ksi)
G_{12}	=	3,448	MPa	(500 ksi)
ν_{12}	=	0.3		
X_T	=	1379	Mpa	(200 ksi)
Y_T	=	345	Mpa	(50 ksi)
Y_C	=	69	Mpa	(10 ksi)
S	=	83	Mpa	(12 ksi)

2.1.1 Fiber Failure Modes.

Fiber Breakage. For fiber breakage to occur, the stress in the fiber direction of the lamina must be tensile. When the fiber breakage failure criterion is satisfied, all of the in-plane elastic constants for that particular lamina are degraded, *i.e.* E_{11}, E_{22}, G_{12}, ν_{12}, and ν_{21}. The elastic constants are degraded over an arbitrary number of time steps (100 time steps were used in this demonstration) until they are equal to zero. Gradual degradation of the elastic constants was implemented to minimize dynamic instabilities associated with sudden load redistribution.

Results from a calculation demonstrating fiber breakage are shown in Figure 11. The calculation was performed on a single-element shell laminate with unidirectional fibers (oriented in the x-direction). Monotonically increasing shear and longitudinal (in the direction of the fibers) strains were applied to the laminate simultaneously. The ratio of the applied shear strain to the applied longitudinal strain was one. Fiber breakage occurs when a combination of the stresses exceeds the fiber breakage strength relation, Equation 12. The failure stresses are $\sigma_{11} = 825$ MPa and $\sigma_{12} = 71$ MPa. After failure, both the stress in the fiber direction and the shear stress are reduced to zero over 100 time steps while the corresponding strains increase. Note that the nonlinearity observed in the shear stress-strain behavior is due to the non-zero shear stress parameter used in the calculation ($\alpha = 3.05 \times 10^{-8}$ MPa^{-3}).

Fiber Compressive Failure. At present, the damage model does not check the compressive stress in the fiber direction to determine if fiber compressive failure would occur. To include such failure, one would have to determine whether or not the failure criterion and post-failure degradation rule depend on the mode of compressive failure. For instance, interactive failure may affect property degradation in the transverse fiber and shear directions, while fiber kinking and subsequent fracture may also affect Young's modulus in the longitudinal-fiber direction.

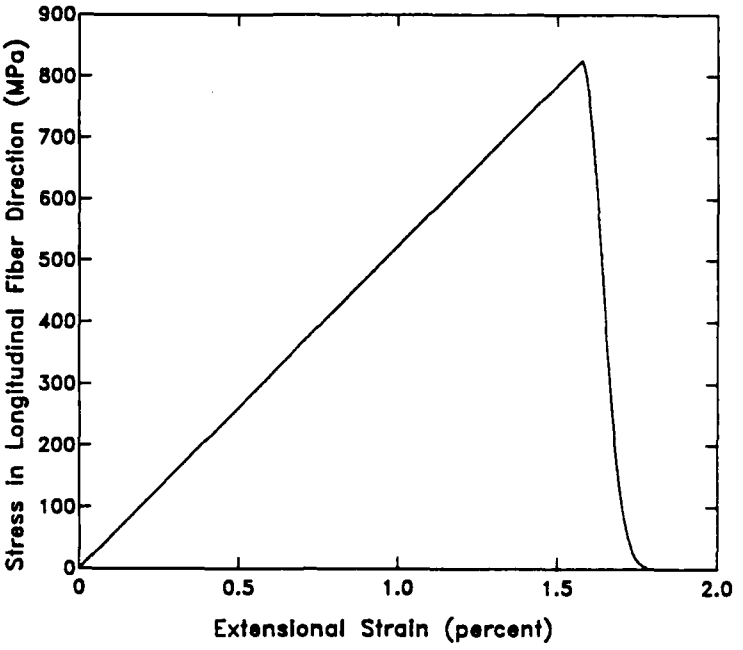

(a) Stress-strain behavior in longitudinal fiber direction.

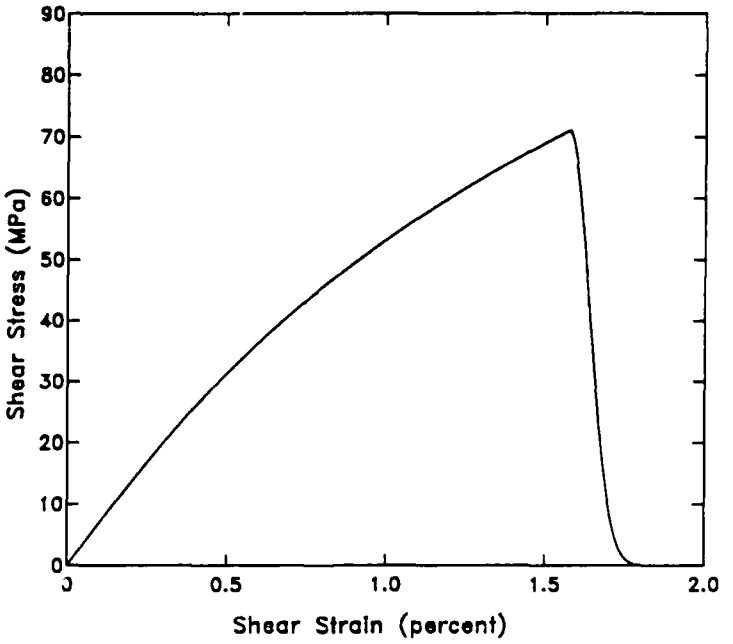

(b) Shear stress-strain behavior.

Figure 11. Demonstration of fiber breakage failure.

2.1.2 Matrix Failure Modes.

Matrix Cracking Failure. For matrix cracking failure to occur, the stress transverse to the fiber direction must be tensile. If the failure criterion is satisfied, the transverse Young's modulus, shear modulus, and both the Poisson's ratios are set to zero for that particular lamina, *i.e.* $E_{22} = G_{12} = \nu_{12} = \nu_{21} = 0$. At present, these moduli are degraded over a single time step. A literature search was performed to determine what degradation rules are appropriate for the matrix failure modes, *i.e.* which elastic constants should be degraded. Results of the literature search and modifications to the DYNA3D implementation are discussed in Section 2.4.

Results from a calculation demonstrating matrix cracking failure are shown in Figure 12. The calculation was performed on a single-element shell laminate with unidirectional fibers (oriented in the x-direction). A monotonically increasing strain was applied in the transverse fiber direction (y direction). A monotonically increasing shear strain was simultaneously applied to the laminate. The ratio of the applied shear strain to applied longitudinal strain was one. A nonlinear shear stress parameter of $\alpha = 3.05 \times 10^{-8}$ MPa^{-3} was used in the calculation. When a combination of the transverse stress and shear stress exceeds the strength relation, Equation 13, matrix cracking failure occurs. The failure stresses are $\sigma_{22} = 130$ Mpa and $\sigma_{12} = 78$ MPa. Both the stress in the transverse fiber direction and the shear stress drop to zero over one time step, while the corresponding strains become large.

Matrix Compression Failure. For matrix compression failure to occur, the stress transverse to the fiber direction must be compressive. If the failure criterion is satisfied, the transverse Young's modulus and both the Poisson's ratios are set to zero for that particular lamina, *i.e.* $E_{22} = \nu_{12} = \nu_{21} = 0$.

Results from a calculation demonstrating matrix compression failure are shown in Figure 13. The calculation was performed on a single-element-shell laminate with unidirectional fibers (oriented in the x-direction). A monotonically increasing compressive strain was applied in the transverse fiber direction (y direction). A monotonically increasing shear strain was simultaneously applied to the laminate. The ratio of the applied shear strain to applied longitudinal strain was minus one. When a combination of the transverse compressive stress and shear stress exceeds the strength relation, Equation 14, matrix compression failure occurs. The failure stresses are $\sigma_{22} = 48$ Mpa and $\sigma_{12} = 48$ MPa. The stress in the transverse fiber direction drops to zero over one time step while the corresponding strain increases. However, the shear stress continues to increase with increasing shear strain because the shear modulus is not degraded in the Chang post-failure degradation rule for matrix compression failure.

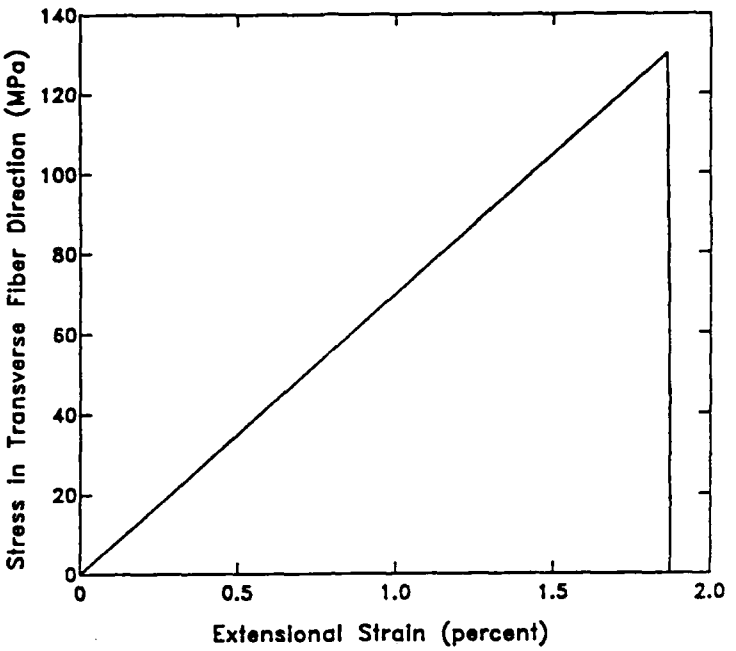

(a) Stress-strain behavior in transverse fiber direction.

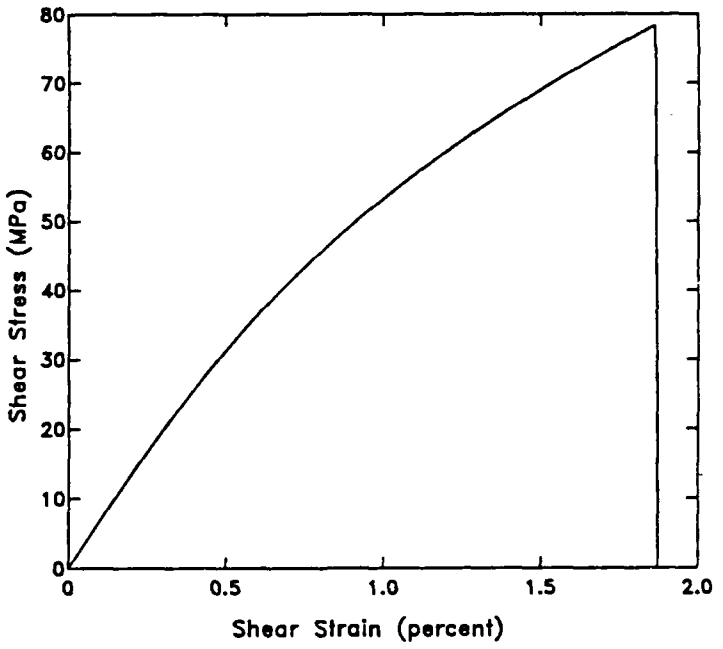

(b) Shear stress-strain behavior.

Figure 12. Demonstration of matrix cracking failure.

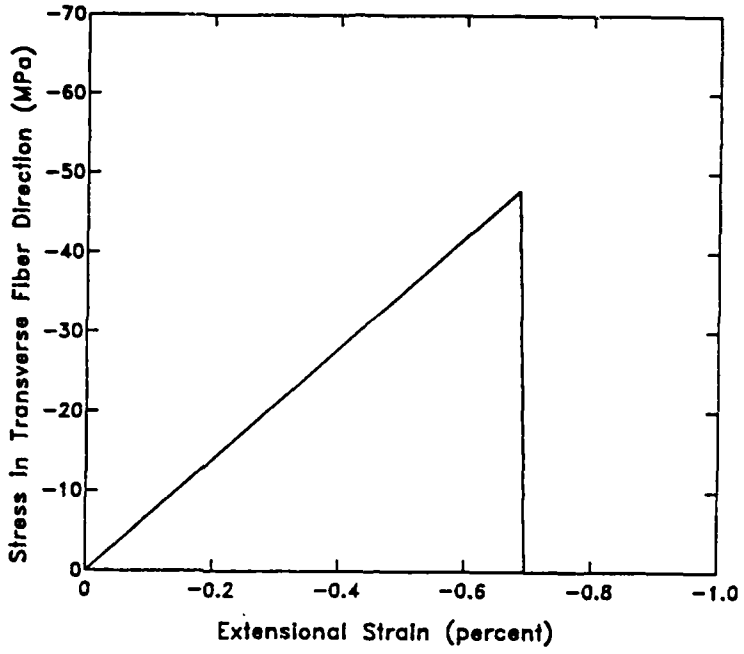

(a) Stress-strain behavior in transverse fiber direction.

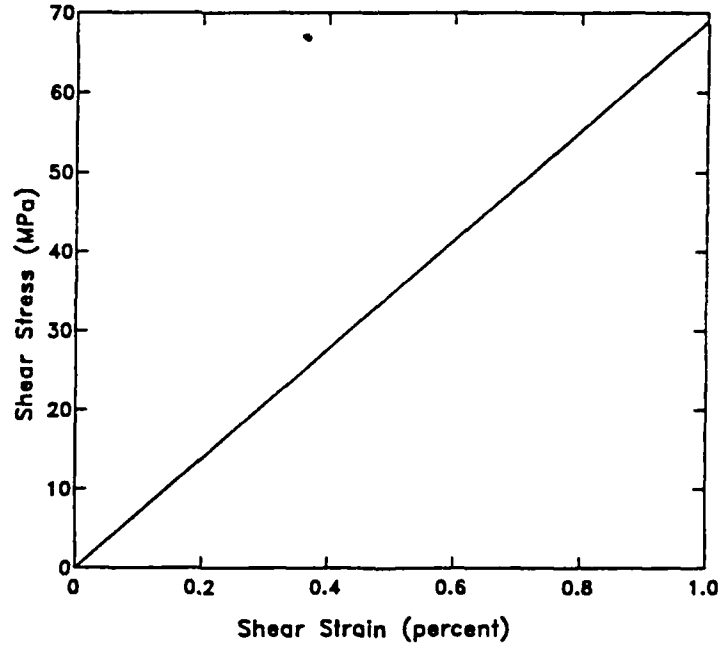

(b) Shear stress-strain behavior.

Figure 13. Demonstration of matrix compression failure.

2.2 CALCULATIONS TO DEMONSTRATE POST-FAILURE BEHAVIOR.

Two calculations were performed to verify the post-failure behavior of cross-ply laminates after initial ply failure. In the first calculation the unloading behavior of a cross-ply laminate was examined using the post-failure degradation rules implemented in APTEK's version of DYNA3D[1]; we are satisfied that the post-failure degradation rules are implemented correctly. In the second calculation the behavior of a cross-ply laminate which exercises a different post-failure degradation rule, *viz.* constant stress after matrix failure, was examined. Comparison of the two calculations indicates that the ultimate strength of the laminate is extremely sensitive to the post-failure behavior assumed for the matrix.

In these two verification calculations, velocities are applied to each node of an element composed of alternating cross-ply lamina to achieve a state of combined extensional and shear strain. The applied extensional strain is in the fiber direction of some of the cross plies and transverse to the fiber direction of the remaining cross plies. The material strength parameters were chosen to demonstrate failure and degradation in each of the tensile failure modes. Failure and material property degradation depend on the fiber orientation of each lamina and the sign of the stress.

2.2.1 Post-Failure Behavior of a Symmetric Cross-Ply Laminate.

Results from a calculation demonstrating fiber breakage with matrix cracking and degradation are shown in Figure 14. The calculation was preformed with the post-failure degradation rules implemented in DYNA3D, *i.e.* instantaneous unloading. This unloading behavior was previously shown in Figures 11 and 12. The calculation was preformed with a three-layer cross-ply laminate, $[90°, 0°, 90°]$, where 0° corresponds to the x direction and 90° corresponds to the y direction of the laminate, as shown in Figure 15. A monotonically increasing strain was applied to the laminate in the x direction, *i.e.* the tensile strain was applied in the fiber direction of the 0° lamina and in the transverse fiber direction of the 90° laminae. A monotonically increasing shear strain was applied simultaneously. The laminate was 2.54-mm-thick with the following tensile strengths:

$$
\begin{array}{lcrll}
X_T & = & 1379 & \text{MPa} & (200 \text{ ksi}) \\
Y_T & = & 34 & \text{MPa} & (\ 5 \text{ ksi}) \\
Y_C & = & 69 & \text{Mpa} & (\ 10 \text{ ksi}) \\
S & = & 83 & \text{MPa} & (\ 12 \text{ ksi})
\end{array}
$$

[1]The constant-stress post-failure degradation rules implemented in DYNA3D were modified by APTEK to allow the shear and/or transverse stresses to degrad instantaneously following matrix failure.

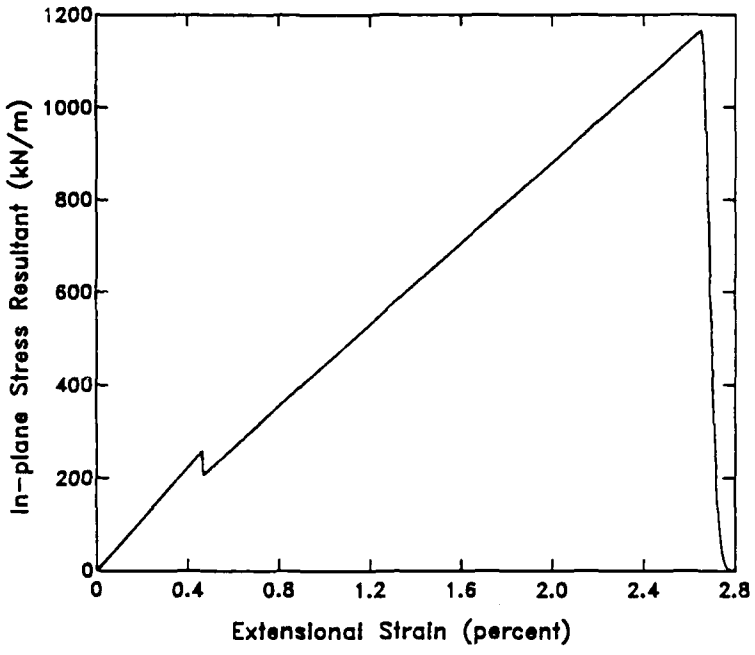

(a) Laminate stress resultant-strain behavior in x direction.

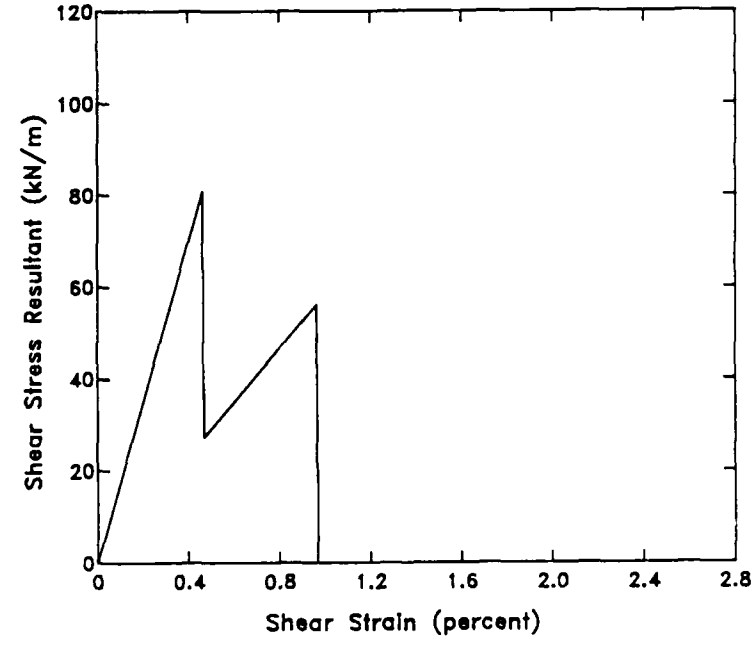

(b) Laminate shear stress resultant-strain behavior.

Figure 14. Demonstration of post-failure behavior in DYNA3D.

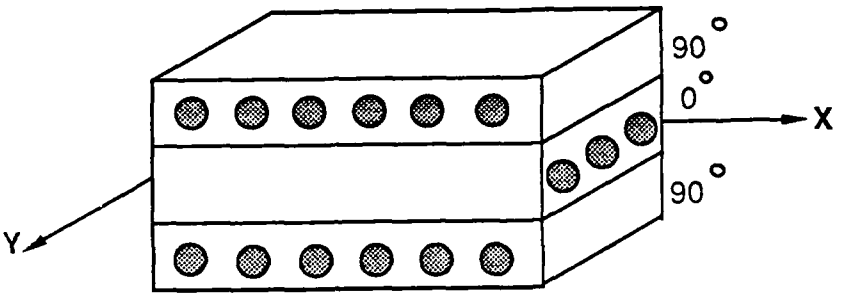

Figure 15. Cross-ply laminate used in post-failure demonstration calculations.

The first failure to occur is matrix cracking in both 90° laminae. Once these lamina fail, the effective modulus of the laminate is reduced because the failed laminae cannot carry any stress in the transverse fiber direction. The change in effective modulus of the laminate is indicated by the drop in the in-plane stress resultant in the x direction, N_x, when $\epsilon_x = 0.46\%$. The effective shear modulus of the laminate is also reduced to one-third its original value because the failed lamina cannot carry any shear stress once matrix cracking failure occurs. The change in effective shear modulus is indicated by the drop in the shear stress resultant, N_{xy}, when $\epsilon_{xy} = 0.46\%$.

After failure of the 90° laminae, stress in the x direction and shear stress must be carried by the 0° lamina. However, all lamina are still able to carry stress in the y direction. As the laminate extends in the x direction, it contracts in the y direction due to the *effective* Poisson's ratio of the laminate. This ratio depends on the elastic constants and orientations of all plies within the laminate and is calculated from the extensional stiffness coefficients of the laminate: $\nu_{xy} = A_{12}/A_{22}$[2]. For the cross-ply laminate used in this example, the effective Poisson's ratio of the laminate, $\nu_{xy} = 0.019$, is less than the Poisson's ratio of the 0° lamina, $\nu_{12} = 0.3$. This mismatch between the Poisson's ratios of the laminate and the 0° lamina causes tensile stresses to develop in the transverse fiber direction of the 0° lamina and compressive stresses to develop in the fiber direction of the 90° lamina; the net laminate stress resultant in the y direction is zero. Matrix cracking failure occurs in the 0° lamina when the transverse tensile stress exceeds the corresponding strength of the material. At this strain level, $\epsilon_x = \epsilon_{xy} \approx 1.0\%$, none of the lamina are able to carry shear stress so the shear stress drops to zero. The effective Poisson's ratio of the laminate is also reduced to zero.

[2]Extensional stiffness coefficients and laminate *effective* moduli are discussed in a previous report to DNA in Reference [28].

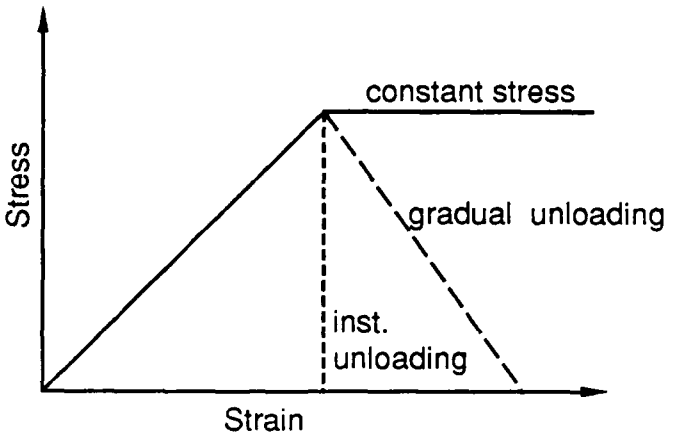

Figure 16. Post-failure degradation behavior in fiber-composite lamina.

The last failure to occur in the laminate is fiber breakage in the 0° lamina. Breakage occurs when the stress in the fiber direction of the 0° lamina exceeds the longitudinal tensile strength of the material.

This calculation demonstrates the implementation of the post-failure degradation rules in DYNA3D. We are not sure that instantaneous unloading for the matrix failure modes is appropriate for all fiber-composite materials. Other possible methods are constant stress after matrix failure (transverse and shear) or gradual decay of the transverse stress and shear stress after the matrix fails, as shown schematically is Figure 16 and discussed in References [17] and [19]. Another method (not shown) is partial reduction of some of the elastic moduli, as discussed in Reference [29].

2.2.2 Effect of Post-Failure Behavior on Ultimate Strength.

In this section we demonstrate how the post-failure behavior of the matrix affects the ultimate strength and stress resultant-strain history of a layered composite. This is done by comparing the calculated response of a cross-ply laminate exhibiting constant stress after matrix failure with the calculated response of a laminate exhibiting instantaneous unloading.

The response of a three-layer cross-ply laminate with instantaneous unloading of the transverse and shear stresses was discussed in the previous subsection. Now consider the same laminate and applied strain history, but allow the transverse and shear stresses to remain constant after matrix cracking failure. Comparisons of stress resultant-strain histories calculated for the two post-failure behaviors are shown in Figure 17.

As previously demonstrated, the first failure to occur is matrix cracking in the 90° lamina, which reduces the effective axial and shear moduli of the laminate. With the

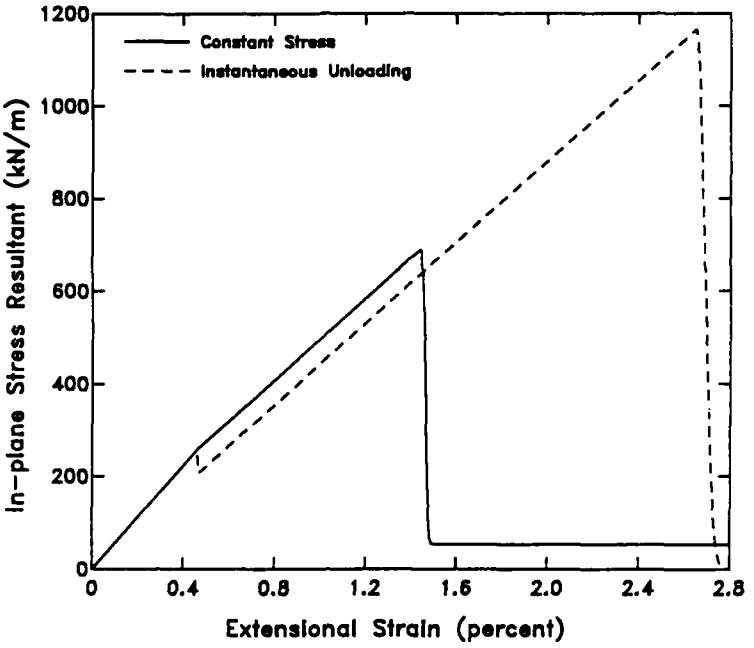

(a) Laminate stress resultant-strain behavior in x direction.

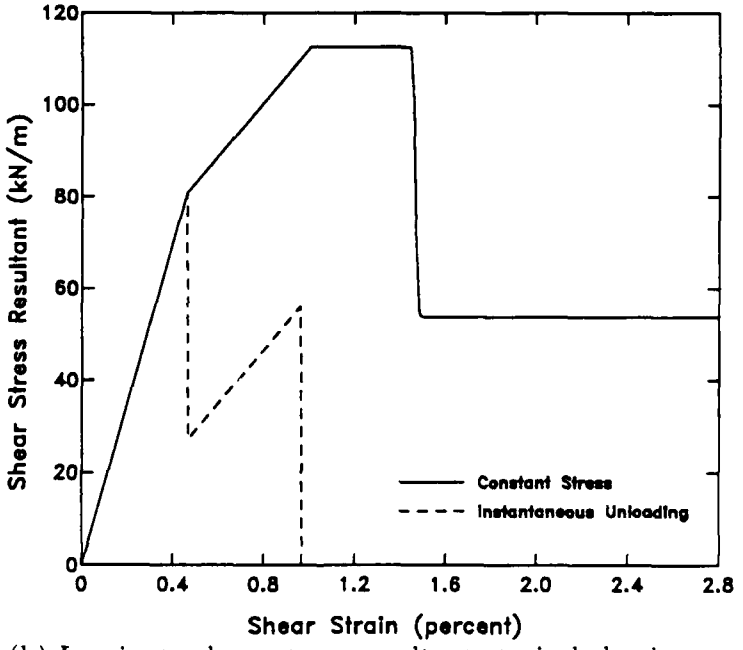

(b) Laminate shear stress resultant-strain behavior.

Figure 17. Comparison of stress resultant-strain behaviors for laminates with different post-failure behaviors.

constant stress degradation rule, the changes in effective moduli of the laminate are indicated by the change in slope of the corresponding stress resultant-strain curves. The matrix continues to carry the transverse and shear stresses at failure, but all *additional* stresses must be carried by the 0° lamina.

Additional strain was applied to the laminate until matrix cracking occured in the 0° lamina due to the mismatch between the Poisson's ratios of the ply and laminate. At this strain, $\epsilon_x = \epsilon_{xy} \approx 1.0\%$, none of the lamina are able to carry *additional* shear load so the shear stress resultant remains constant with increasing shear strain until fiber breakage occurs. Fiber breakage occurs when a combination of the increasing longitudinal stress and constant shear stress exceeds the strength of the 0° lamina at $\epsilon_x = \epsilon_{xy} = 1.46\%$.

Note that the maximum in-plane stress resultant calculated with the constant stress unloading assumption is only $N_x = 699$ kN/m (3992 lb/in). This value is 40% lower than the in-plane stress resultant calculated with instantaneous unloading of the matrix, which is $N_x = 1169$ kN/m (6675 lb/in). The constant stress unloading value is lower because the matrix continued to carry shear stress after matrix failure, and shear stress is assumed to weaken the composite and contribute to fiber breakage in the Chang fiber breakage failure criterion. These comparative examples indicate that the calculated response and ultimate strength of a laminate with matrix failure are very sensitive to the post-failure behavior of the matrix.

2.3 COMPARISON OF FAILURE CRITERIA WITH EXPERIMENTAL RESULTS.

In this section, numerical results are compared with experimental results available in the literature to establish the validity of the Chang failure criteria implemented in DYNA3D. Three sets of material property tests are analyzed: lamina off-axis tests to verify the tensile failure criteria (fiber and matrix), lamina combined stress tests to verify the matrix failure criteria, and biaxial stress tests on quasi-isotropic laminates to verify the fiber failure criteria.

Results presented in this section indicate that the Chang matrix tensile failure criterion is in fair agreement with lamina off-axis test data. The Chang fiber breakage criterion is also in fair agreement with failure strengths measured from two off-axis tests, although two data points are not enough to validate the criterion. Comparison of the fiber failure criterion with biaxial stress tests on quasi-isotropic laminates was inconclusive in validating the Chang fiber breakage failure criterion. Comparison of the matrix failure criteria with combined stress test data indicate that the Chang matrix tensile and compressive failure criteria implemented in DYNA3D do not adequately model matrix strength under combined loading conditions. A modified form of the Tsai-Wu criterion is in better agreement with the test data and is therefore recommended for implementation in DYNA3D.

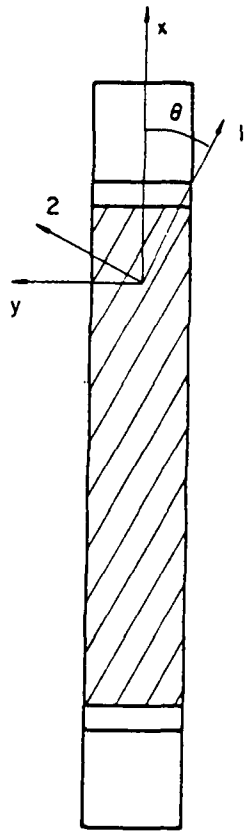

Figure 18. Geometry of the off-axis tensile specimen.

2.3.1 Lamina Off-Axis Tests.

Lamina tensile strength is often characterized by performing uniaxial tests on unidirectional specimens with fibers oriented at-angle to the loading axis, as shown in Figure 18. The measured strength depends on the off-axis angle, θ, between the fiber direction and loading axis. Extensional-shear coupling occurs when fibers are oriented at-angle to the loading axis.

The theoretical tensile strength of the specimen is determined from the Chang fiber breakage and matrix cracking criteria. This is done by transforming the applied axial stress, σ_x, into stresses in the principal material directions of the lamina, as follows:

$$\begin{bmatrix} \sigma_1 \\ \sigma_2 \\ \sigma_{12} \end{bmatrix} = \sigma_x \begin{bmatrix} m^2 \\ n^2 \\ -mn \end{bmatrix} \tag{15}$$

where $m = \cos\theta$, $n = \sin\theta$, and θ is the orientation angle between the fiber direction and loading axis. The state of stress in the fiber coordinate system is biaxial. The

maximum applied stress is found by substituting the lamina stresses from Equation 15 into the fiber breakage and matrix cracking criteria, Equations 12 and 13 respectively:

$$\text{Fiber Breakage}: \quad \sigma_x|_{\text{fiber}} = \left[\left(\frac{m^2}{X_T}\right)^2 + \left(\frac{mn}{S}\right)^2\right]^{-1/2} \tag{16}$$

$$\text{Matrix Cracking}: \quad \sigma_x|_{\text{matrix}} = \left[\left(\frac{n^2}{Y_T}\right)^2 + \left(\frac{mn}{S}\right)^2\right]^{-1/2} \tag{17}$$

Equations 16 and 17 give the ultimate tensile strengths for fiber breakage, $\sigma_x|_{\text{fiber}}$, and matrix cracking, $\sigma_x|_{\text{matrix}}$, versus off-axis angle. These equations are plotted in Figure 19 for a graphite-epoxy specimen.

For small angles, the ultimate strength calculated for fiber breakage is less than that for matrix cracking. For larger angles, the ultimate strength calculated for matrix cracking is less than that for fiber breakage. The orientation angle which separates the fiber and matrix modes is found by setting the ultimate strength for fiber breakage equal to the ultimate strength for matrix cracking, $\sigma_x|_{\text{fiber}}=\sigma_x|_{\text{matrix}}$, which gives the following separation angle:

$$\theta = \tan^{-1}\left(\frac{Y_T}{X_T}\right)^{\frac{1}{2}} \tag{18}$$

This separation angle is $\theta = 8.8°$ for graphite-epoxy with $X_T = 1980$ MPa and $Y_T = 48$ MPa.

Strengths measured from an off-axis test on a graphite-epoxy specimen are compared with the Chang tensile failure criteria in Figure 19. The data were obtained from Reference [30, p. 115]. There is good agreement between the test data and the tensile failure criteria implemented in DYNA3D. The fiber breakage criterion is in agreement with the test data for angles less than the separation angle while the matrix cracking criterion is in agreement with the test data for angles greater than the separation angle. Although the mode of failure was not reported for the test data, the comparisons suggest that the tests were terminated once matrix tensile failure occured in the lamina for angles greater than the separation angle.

The test data also indicate that the ultimate strength of the off-axis specimen tested at 5° is 60% less than a specimen tested at 0°. However, this test does not validate the fiber breakage failure criterion in DYNA3D for two reasons. First, the observed failure mode was not reported for the data, so we do not know if fiber or matrix failure occured at 5°. Second, longitudinal fiber, transverse fiber, and shear stresses act on the composite in the fiber coordinate system, but only shear and longitudinal stress are assumed to contribute to fiber breakage in the Chang failure criterion. Shear stress is assumed to cause fiber-matrix debonding, thus reducing the longitudinal tensile strength. However, stress in the transverse fiber direction could also cause matrix cracking failure, which may also contribute to a reduction in longitudinal tensile strength. The relative effects of the transverse (σ_{22}) and shear

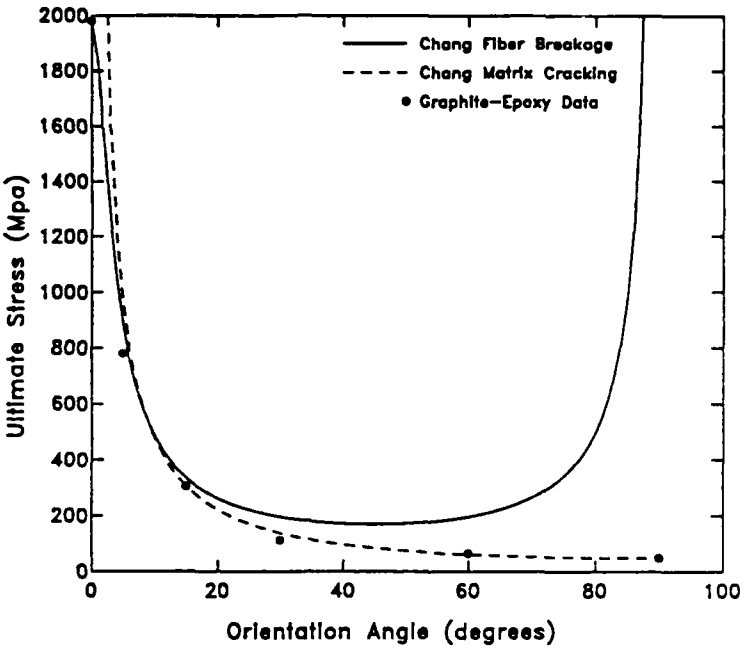

Figure 19. Ultimate tensile strength versus off-axis angle for unidirectional tensile test specimens.

(σ_{12}) stresses on the reduction in longitudinal tensile strength are not established. *Note:* it could also be argued that the matrix cracking criterion is not adequately verified because the relative effects of σ_{11} and σ_{12} on matrix cracking failure are not established.

The same graphite-epoxy test data are compared with two commonly used failure criteria, the Tsai-Wu and maximum stress criteria, in Figure 20. This was done to determine how the form of the failure criteria affects the shape of ultimate strength versus off-axis angle curve. The Tsai-Wu criterion is a single smooth curve in ultimate stress versus orientation-angle space, and is in excellent agreement with the data. The maximum stress criteria consists of three intersecting curves which correspond to longitudinal fiber tensile failure, transverse tensile failure, and shear failure. The maximum stress criteria are also in good agreement with the data, although the maximum stress criteria overestimate the strength of the laminate at 30° because interaction between the in-plane shear and transverse stress components are not taken into account. In conclusion, differences between the Chang, Tsai-Wu, and maximum stress criteria are not readily apparent when the failure curves are plotted in ultimate strength versus orientation-angle space.

Another way to compare off-axis test data with failure criteria is in lamina stress (σ_{11} , σ_{22} , σ_{12}) space. This comparison provides a more exacting assessment of the criteria than the ultimate strength *vs.* orientation angle plots, particularly for intermediate orientation angles where failure occurs in the matrix and is dominated by

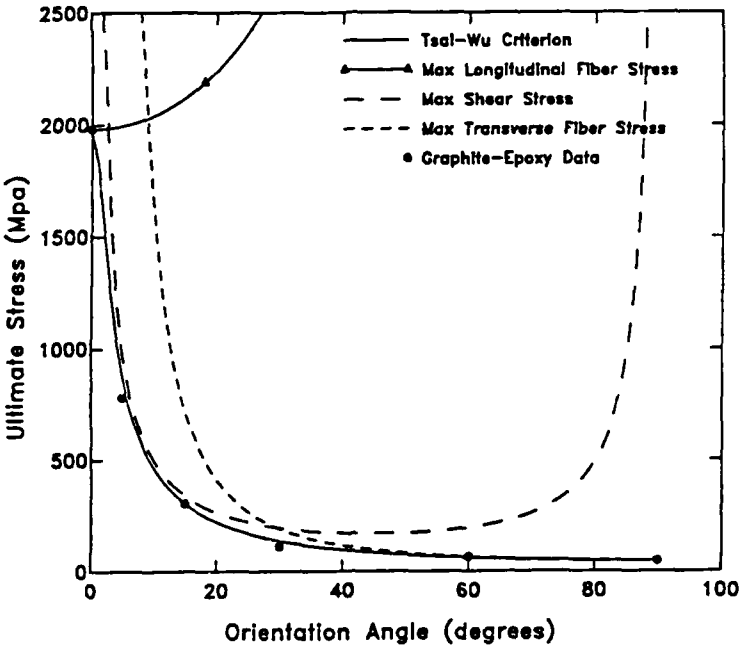

Figure 20. Comparison of the Tsai-Wu and maximum stress criteria with data from off-axis test specimens.

σ_{12} and/or σ_{22}. These stresses, σ_{12} and σ_{22}, are small compared to the maximum ordinate of the ultimate stress *vs.* orientation angle plot, which is $\sigma_x \approx X_T$.

For the Chang criteria, comparisons in stress space are easy to visualize because failure by fiber breakage or matrix cracking are each associated with surfaces parallel to one of the stress axes (cylindrical surfaces), defined by Equations 12 and 13. The only difficulty, as previously mentioned, is that one must know which mode each specimen failed in to plot its data point for comparison with the appropriate failure surface. Comparisons are shown in Figures 21 and 22 with the assumption that failure occured by fiber breakage for $\theta < 8.8°$, and by matrix cracking for $\theta > 8.8°$. Figures 21 and 22 can be visualized looking down the axis of each cylindrical failure surface. Thus, the distance from a test data point to the surface is seen as a true length. To help interpret these figures, measured failure stresses in the principal material directions of the lamina are listed in Table 4.

Figure 21 shows fiber failure data plotted in a σ_{11} , σ_{12} projection, with the associated end view of the Chang fiber breakage cylindrical failure surface. The data point for $\sigma_{12} = 0$ ($\theta = 0$) lies exactly on the surface because the data from this test was used in establishing the surface. The shear strength of 85 MPa at $\sigma_{11} = 0$ completed the surface definition and was obtained from tensile test data on $\pm 45°$ lamina specimens (Reference [30], p. 63). The other fiber failure point from the off-axis tests at $\theta = 5°$ lies below the surface by a more readily apparent distance than in the ultimate strength plot in Figure 19.

Table 4. Graphite-epoxy off-axis test data.

θ (degrees)	σ_x (MPa)	σ_{11} (MPa)	σ_{22} (MPa)	σ_{12} (MPa)
0	1980	1980	0	0
5	780	774	6	68
15	305	284	20	76
30	112	84	28	48
60	65	16	49	28
90	48	0	48	0

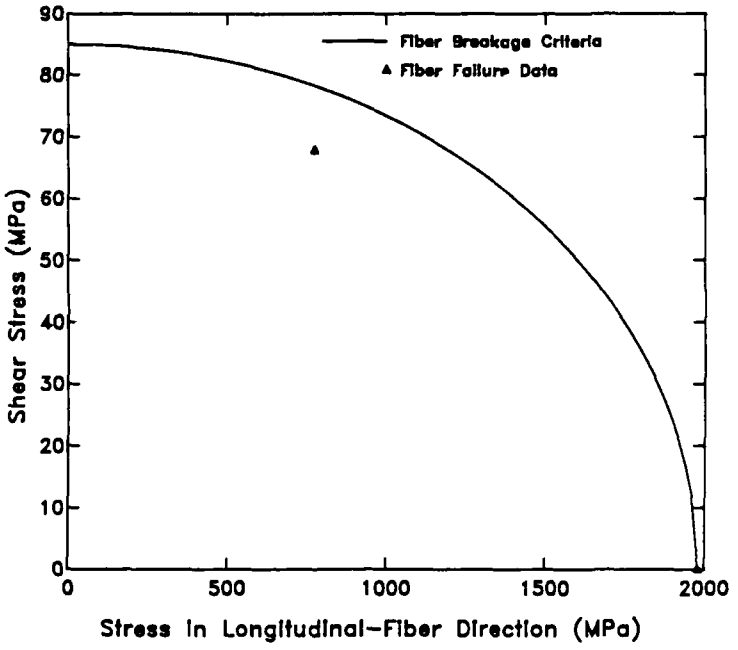

Figure 21. Comparison of off-axis test data with Chang fiber breakage criterion.

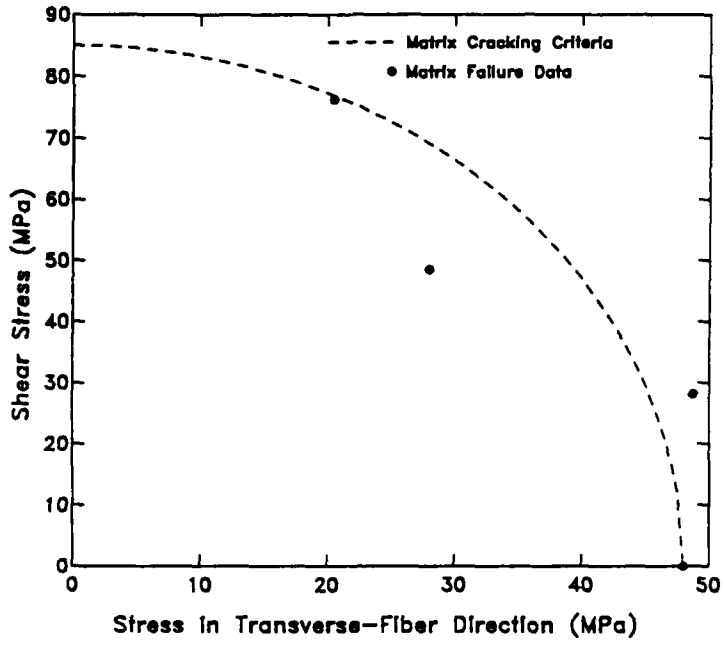

Figure 22. Comparison of off-axis test data with Chang matrix cracking criterion.

Figure 22 shows matrix failure data plotted in a σ_{22}, σ_{12} projection along with the associated end view of the Chang matrix failure cylindrical surface. Again, the data point for $\sigma_{12} = 0$ lies exactly on the surface, because it was used to establish the surface. The important observation here is that the data point measured at 30° ($\sigma_{22} = 28$ MPa, $\sigma_{12} = 48$ MPa) falls substantially off the failure surface when viewed along the σ_{11} stress axis, because the large value of $\sigma_x = X_T$ does not dominate the comparison as it does in the ultimate strength plot in Figure 19.

Conclusions.

The Chang fiber breakage and matrix cracking criteria are only in fair agreement with the test data when the data are plotted in stress space. The two data points in Figure 21 are not enough to validate the fiber breakage criterion. In addition, the effects of σ_{22} on fiber breakage failure and σ_{11} on matrix cracking failure are not adequately addressed in these tests. Additional biaxial characterization data of composite specimens is needed to validate both the Chang fiber and matrix tensile failure criteria. Additional biaxial tests are discussed in the following two subsections.

2.3.2 Fiber Failure Modes Under Biaxial Stress.

Swanson *et al.* in References [31-34] reported biaxial stress experiments on quasi-isotropic carbon-epoxy (AS4/3501-6) laminates, $[90°, \pm 45°, 0°]_S$. Fiber failure data were obtained from static tests on thin-walled cylindrical tubes under combined internal pressure and axial load (both tension and compression). The failure data are

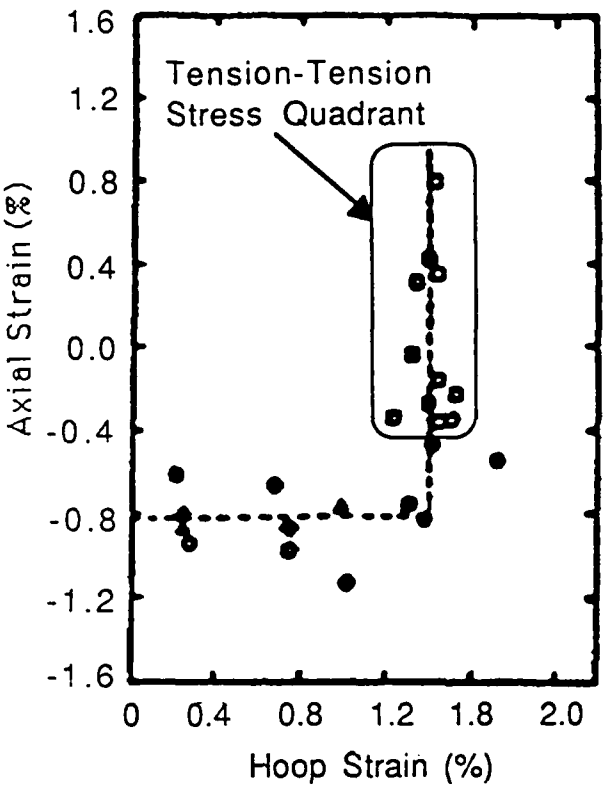

Figure 23. Failure strain data for a quasi-isotropic carbon-epoxy laminate under biaxial stress.

shown in Figure 23 for combinations of hoop and axial strain. The average hoop failure strain from all tubes tested in tension-tension (axial tension combined with hoop tension) is 1.40%. This average failure strain is close to a value of 1.46% measured by Swanson in unidirectional tensile coupon tests. Swanson *et al.* concluded that the tensile hoop failure strain is constant at failure and independent of the applied stress state, at least in the tension-tension stress quadrant.

Swanson *et al.* in Reference [32] also reported combinations of hoop and axial stress which produced failure in the laminate. They compared the failure stress data with failure stress envelopes calculated using the maximum fiber strain criterion and the Tsai-Wu failure criterion. These failure envelopes are compared with the test data in Figure 24 for the tension-tension stress quadrant only. Two envelopes are shown for the maximum strain criterion. The dashed envelope is calculated with linear laminated plate theory (LPT) and the solid v-shape line is calculated with a progressive softening model that includes nonlinear shear behavior and reduction in ply stiffness[3] due to matrix cracking. The maximum strain criterion with progressive softening agrees best with the measured data, although the maximum strain criterion without the degradation model is also in reasonable agreement with the data. The Tsai-Wu criterion is in poor agreement with the data. With the Tsai-Wu criterion.

[3]Swanson and Christoforou in Reference [32] use a gradual degradation rule to model the reduction in transverse Young's modulus, E_{22}, as a function of transverse strain.

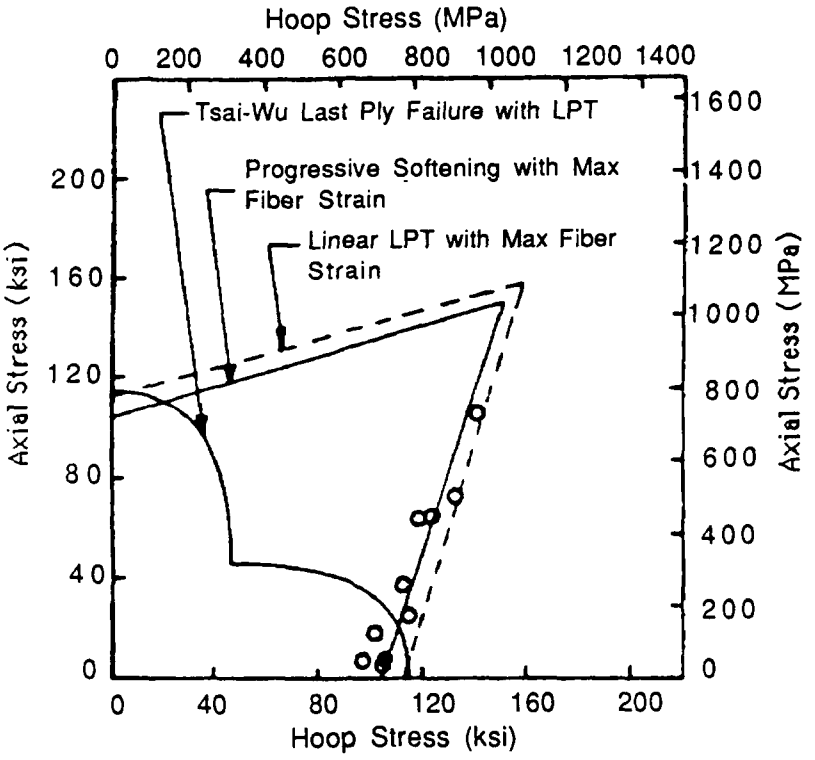

Figure 24. Laminate failure envelopes calculated with the Tsai-Wu and maximum strain criteria for a quasi-isotropic carbon-epoxy laminate under biaxial stress.

'last ply' laminate failure occurs when the Tsai-Wu criterion is satisfied for all plies. These results suggest that fiber failure is not adequately modeled by the Tsai-Wu criterion under biaxial stress conditions.

Swanson *et al.* did not report whether fiber failure initiated in the hoop, axial, or at-angle plies. Therefore, the test data are interpreted, in the present report, by calculating the failure envelopes for the individual lamina. Failure envelopes are calculated for two different failure criteria: the maximum stress criterion, and an interactive failure criterion. The failure envelope for the entire laminate is determined from the failure envelopes for the individual lamina. Results from these calculations are discussed in the following paragraphs.

Maximum Stress Failure Criteria.

Combinations of hoop and axial stress which satisfy the maximum stress criterion for fiber failure are shown in Figure 25. For each lamina, fiber failure is bounded by parallel lines in stress space. For example, two straight lines are shown for the axial lamina: one for fiber tensile failure and the other for fiber compression failure. The semi-infinite region bounded by these lines represents the stress states the axial lamina can sustain without fiber tensile or compressive failure occuring. The hoop and $\pm 45°$ laminae fail in fiber compression outside the range of this figure.

Failure in the laminate is the minimum *interaction diagram* of the individual plies.

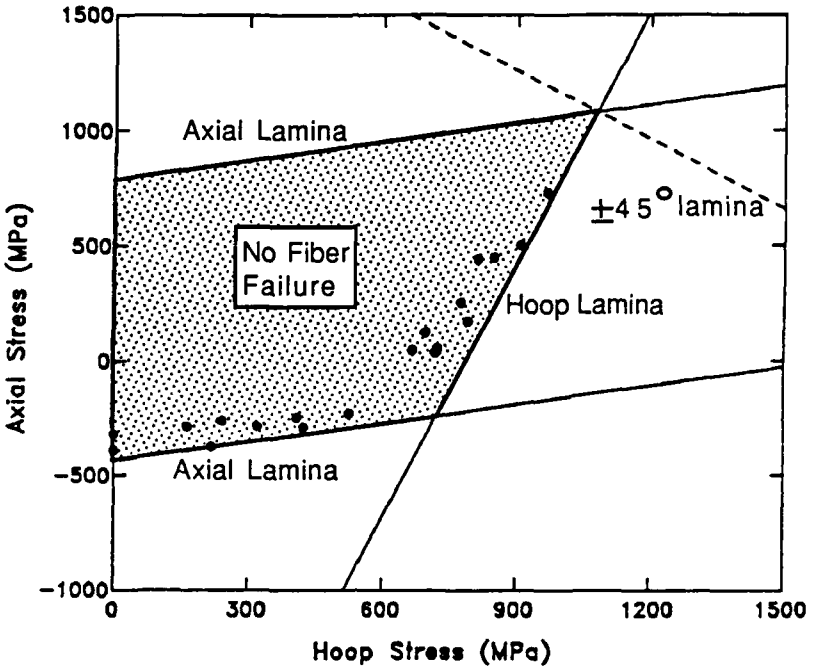

Figure 25. Laminate failure envelope calculated with the maximum stress criterion for a quasi-isotropic carbon-epoxy laminate under biaxial stress.

The shaded area represents the biaxial stress states which the laminate can sustain without fiber failure occurring in any lamina. The shaded area is bounded by the fiber tensile failure curve for the hoop lamina, and the fiber tensile and compressive failure curves for the axial lamina. The laminate failure envelope is in good agreement with the test data, shown as dots in Figure 25, reported by Swanson *et al.*

Note: The following lamina properties and strengths were reported by Swanson in Reference [32] and used in the calculations: $E_{11} = 131$ GPa, $E_{22} = 11.2$ GPa, $\nu_{12} = 0.28$, $X_T = 1950$ MPa. Lamina compressive strength and in-plane shear modulus and strength were not reported. A compressive strength of $X_C = 1074$ MPa was estimated from the measured biaxial stress data. A shear modulus of $G_{12} = 6600$ MPa was calculated using laminated plate theory, the lamina elastic constants, and laminate stiffness measurements reported in Reference [32]. A shear strength of $S = 52$ MPa was estimated from data for AS4/55A carbon-epoxy, which was reported in Reference [35]. Reference [36] reports shear strengths ranging from about 40 MPa for T300/5208 carbon-epoxy tape to 125 MPa for AS4/3502 carbon-epoxy tape at room temperature.

Interactive Failure Criterion.

Failure envelopes were also calculated using an interactive criterion of the following form:

$$\left(\frac{\sigma_{11}}{X}\right)^2 + \left(\frac{\sigma_{12}}{S}\right)^2 \geq 1 \tag{19}$$

where X is the longitudinal fiber strength in either tension or compression. For fiber tensile failure ($\sigma_{11} > 0$), $X = X_T$, and Equation 19 reduces to the Chang fiber breakage criterion. For fiber compressive failure ($\sigma_{11} < 0$), $X = X_C$ in Equation 19; this fiber compressive failure criterion is suggested by Humphreys and Rosen in Reference [37].

Combinations of hoop and axial stress which satisfy the interactive criterion for fiber failure are shown in Figure 26. For the hoop and axial lamina, fiber failure is bounded by parallel lines in stress space, in agreement with those calculated from the maximum stress criterion. This is because the shear stress in the principal material directions of the hoop and axial lamina is zero. Fiber failure occurs when the stress in the longitudinal fiber direction exceeds the corresponding strength, *i.e.* the interactive criterion reduces to the maximum stress criterion when the shear stress is zero.

For the $\pm 45°$ plies, the shear stress in the principal material directions is not zero. Hence the lamina failure envelope calculated with the interactive criterion, Equation 19, is an ellipse in stress space. Tensile or compressive fiber failure occurs in the at-angle plies for stress states outside the region bounded by the ellipse. Note that the elliptical failure envelope for the at-angle plies is contained almost entirely within the region bounded by the hoop and axial lamina. The portion of the elliptical failure envelope that extends outside the bounds for tensile failure in the hoop and axial lamina is shown as a dashed line.

Failure in the laminate is the minimum interaction diagram of the individual plies. The shaded area is bounded by the laminate failure envelope. Outside the shaded area are the stress states for which fiber tensile or compressive failure occured in at least one lamina. Note that this area is bounded almost entirely by the failure envelopes for the $\pm 45°$ plies (the ellipse).

The laminate failure envelope calculated from the interactive failure criterion is not in good agreement with the test data. The calculated failure strength of the laminate is strongly influenced by the shear stress and strength of the at-angle lamina. It is possible that the shear strength used in the calculation is not in agreement with that of the test specimens, *e.g.* a shear strength of 100 MPa (not shown) gives better agreement with the data. It is also possible that matrix cracking occured in the at-angle plies, which would reduce the value of the shear modulus, and hence reduces the tendency for fiber breakage in the $\pm 45°$ plies. Swanson *et al.* reported that the measured stress-strain response of the laminate shows a small reduction in laminate stiffness at higher stress levels, which they attributed to matrix failure. The results from a sample calculation with the shear modulus reduced to half its original value are shown in Figure 27. With $G_{12} = 3300$ MPa, the laminate failure envelope is in better agreement with the test data. With the shear modulus reduced to $G_{12} = 0$, the failure envelope calculated with the maximum stress failure criterion is obtained.

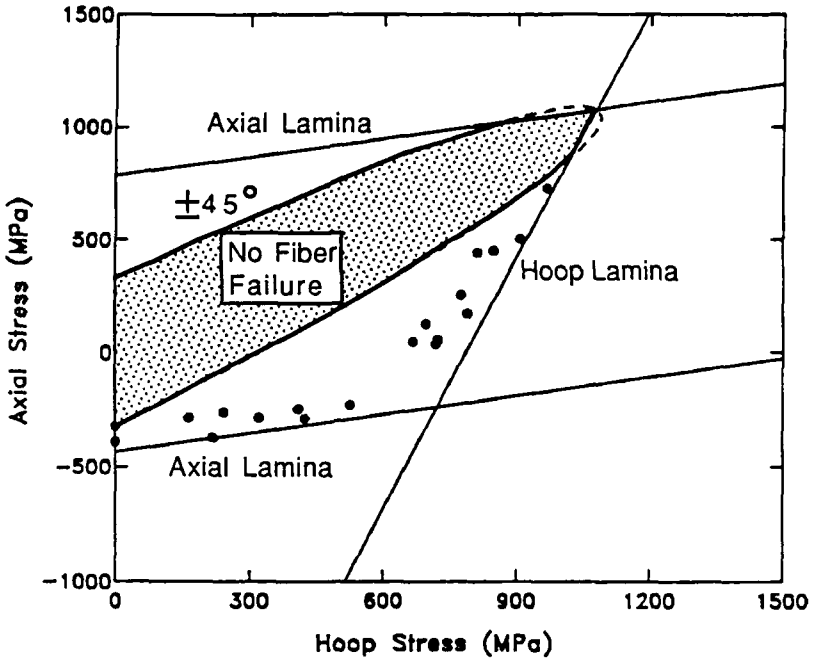

Figure 26. Laminate failure envelope calculated with an interactive failure criterion for a quasi-isotropic carbon-epoxy laminate under biaxial stress.

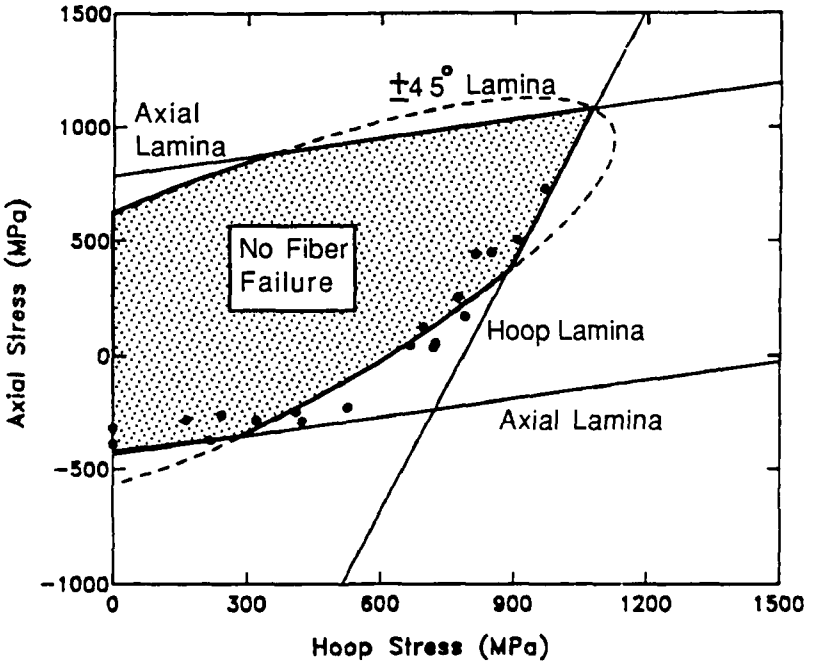

Figure 27. Laminate failure envelope calculated with an interactive failure criterion and a reduced shear modulus.

Conclusions.

Comparisons between the test data and laminate failure envelopes in Figure 26 and 27 are not definitive in validating the interactive failure criterion: the comparisons neither refute nor support the data. The comparisons do not refute the interactive criterion if the shear modulus is reduced to account for matrix cracking failure in the at-angle plies. On the other hand, the comparisons do not support the interactive criterion because the contribution to fiber failure from shear stress is reduced by matrix cracking, so the full effect of the shear stress term in Equation 19 is not validated. In fact, the maximum stress criterion, which neglects the contribution of shear stress to fiber failure, is also in good agreement with the test data. Additional test data are needed to validate the interactive criterion, such as biaxial test data on unidirectional specimens under combined longitudinal fiber stress and shear stress. In particular, we want to validate the Chang fiber breakage criterion[4] implemented in DYNA3D, and validate a fiber compressive failure criterion for future implementation into DYNA3D.

The analyses completed to date also indicate the need to accurately establish the reduction in lamina properties with matrix cracking failure, particularly the post-failure implementation in DYNA3D. Comparisons of the DYNA3D post-failure degradation rules with experimental results available in the literature are discussed in Section 2.4.

2.3.3 Matrix Failure Modes Under Combined Stress.

Swanson, Messick, and Tian in Reference [35] reported failure strengths of carbon-epoxy lamina under conditions of combined transverse-fiber and shear stress. Combined torsion and axial load (both tension and compression) tests were conducted using unidirectional hoop-wound tubes. Tube tests help to minimize free edge delamination and end condition (gripping method) effects which are present in flat test specimens.

Matrix failure data for carbon-epoxy are shown in Figure 28. Transverse tensile and compressive failure stresses are plotted as a function of shear stress. The data show a strong interaction between strength in the transverse fiber direction and shear strength. Note that the shear strength measured with moderate transverse compressive stress is greater than the pure shear strength: the shear strength is approximately 73 MPa for $\sigma_{22} = -50$ MPa while the shear strength is 52 MPa for $\sigma_{22} = 0$ MPa.

Combinations of transverse fiber and shear stress which satisfy the Chang matrix

[4] Analysts who use DYNA3D should be aware of the extent to which shear stress contributes to fiber breakage in the Chang criterion. Currently, fiber breakage is calculated in DYNA3D when a pure shear load is applied to a laminated shell element. However, the criterion is intended to calculate fiber breakage in composites loaded primarily in the longitudinal-fiber direction. Shear stress contributes to fiber breakage by weakening the fiber-matrix interface or through shear failure in the matrix.

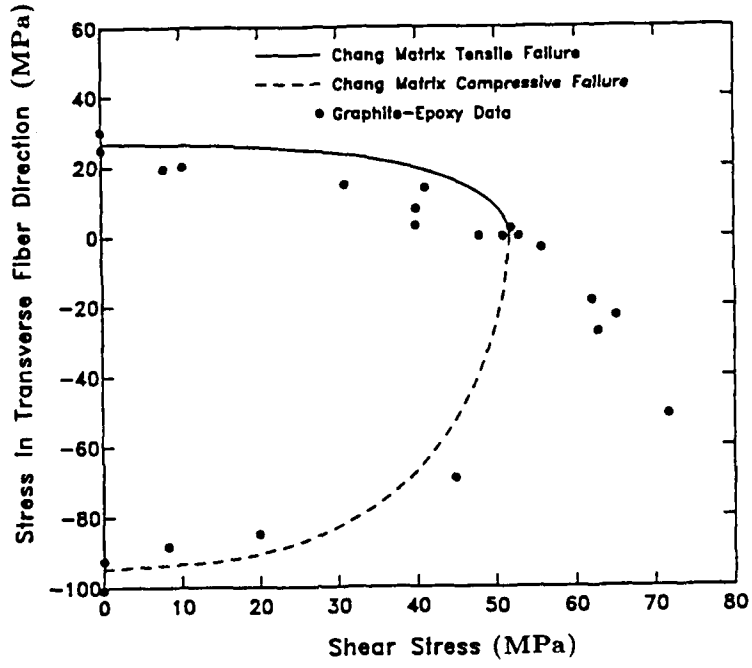

Figure 28. Comparison of Chang matrix failure criteria with matrix failure data for carbon-epoxy.

tensile and compressive failure criteria[5] are also plotted in Figure 28. The calculated tensile failure curve overestimates the tensile strength under combined load conditions. The calculated compressive failure curve is in fair agreement with the test data for large transverse compressive stresses but does not predict the increase in shear strength with moderate compressive stress observed in the test data.

Because of the poor agreement between calculated and measured strengths in Figure 28, a study was performed to determine if other combinations of Y_C and S provide better agreement. The Chang matrix compressive failure criterion[6], Equation 14, is repeated here to aid the discussion:

$$\left(\frac{\sigma_{22}}{2S}\right)^2 + \left[\left(\frac{Y_C}{2S}\right)^2 - 1\right]\frac{\sigma_{22}}{Y_C} + \left(\frac{\sigma_{12}}{S}\right)^2 \geq 1 \qquad (\sigma_{22} < 0) \tag{20}$$

The matrix compression failure criterion contains a linear stress term whose sign depends on the magnitude of the uniaxial compressive strength, Y_C, and the shear strength, S. Equation 20 describes an ellipse in stress space: one-fourth of the ellipse is shown in Figure 29 for three combinations of Y_C and S. When $Y_C = 2S$, the coefficient of the linear stress term is zero and the axes of the ellipse coincide with the coordinate axes (σ_{22} and σ_{12} axes). The maximum shear stress occurs when $\sigma_{22} = 0$.

[5] Uniaxial strengths and properties from Reference [35] were used to calculate the failure surfaces: Y_T = 27 Mpa, Y_C = 95 MPa, and S=52 MPa, G_{12} = 4300 MPa, and $\alpha = 6.88e-08$ MPa^3.

[6] The nonlinear shear stress parameter, α, has been set to zero in Equation 14 to simplify the analysis.

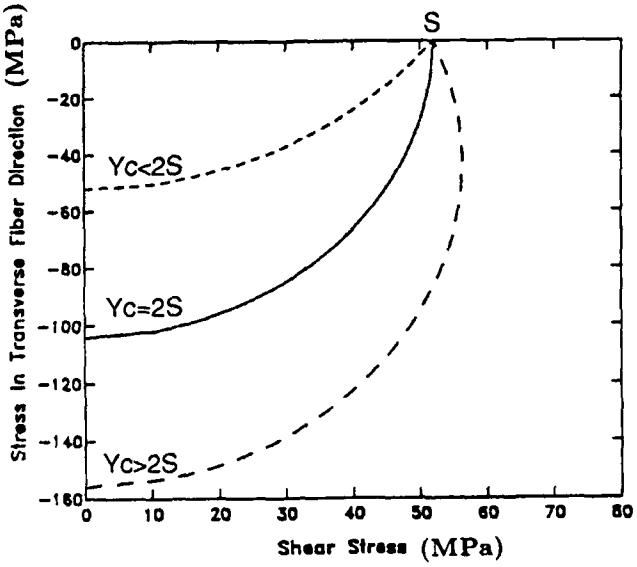

Figure 29. Chang matrix compression failure envelope calculated from three combinations of transverse compressive strength, Y_C, and in-plane shear strength, S.

When $Y_C \neq 2S$, one axis of the ellipse is parallel to the σ_{12} coordinate axis, but does not coincide with the σ_{12} axis. When $Y_C < 2S$, the maximum shear stress occurs when the transverse stress is tensile (not shown). When $Y_C > 2S$, the maximum shear stress occurs when the transverse stress is compressive. This behavior, *i.e.* an increase in shear strength with transverse compressive stress, is observed in the measured data in Figure 28.

The maximum shear stress is determined by maximizing σ_{12} in Equation 20 with respect to σ_{22}. The maximum shear strength under combined loading, $S_{\max}$, is:

$$S_{\max} = S\left[\frac{1}{2} + \left(\frac{Y_c}{4S}\right)^2 + \left(\frac{S}{Y_C}\right)^2\right] \tag{21}$$

The shear strength is a maximum when the compressive stress is:

$$\sigma_{22} = -\left[\frac{{Y_c}^2 - 4S^2}{2Y_C}\right] \tag{22}$$

Equations 21 and 22 are valid for any combination of Y_C and S. Note that when $Y_C >> 2S$, the maximum shear stress attains its largest values as $\sigma_{22} \Rightarrow -Y_C/2$.

The measured shear strength under combined loading in Figure 28 is about 1.45 times the pure shear strength. Substitution of $S_{\max} = 1.45\,S$ into Equation 21 gives $Y_C = 5\,S$. This combination of Y_C and S (not shown) still does not fit the measured

data well. Although the Chang matrix compression failure criterion allows for increased shear strength with transverse compressive stress, a good fit to the measured data cannot be obtained with any reasonable combinations of Y_C and S. Two modifications to the matrix compression failure criterion implemented in DYNA3D are suggested in the following paragraphs.

Hashin Matrix Compression Failure Criterion.

One modification of the Chang matrix compression failure criteria is to include the transverse shear strength. As discussed in Section 1.3, the Chang matrix compressive failure criterion is a modification of the Hashin criterion. Hashin derived his two-dimensional criterion in terms of both the in-plane shear strength, S, and the transverse shear strength, S_T, as follows:

$$\left(\frac{\sigma_{22}}{2S_T}\right)^2 + \left[\left(\frac{Y_C}{2S_T}\right)^2 - 1\right]\frac{\sigma_{22}}{Y_C} + \left(\frac{\sigma_{12}}{S}\right)^2 \geq 1 \quad (\sigma_{22} < 0) \tag{23}$$

This criterion is easily modified to include nonlinear shear behavior following the method of Chang, as follows:

$$\left(\frac{\sigma_{22}}{2S_T}\right)^2 + \left[\left(\frac{Y_C}{2S_T}\right)^2 - 1\right]\frac{\sigma_{22}}{Y_C} + \bar{\tau} \geq 1 \quad (\sigma_{22} < 0) \tag{24}$$

Transverse shear strength is not reported for the carbon-epoxy data in Reference [35]. If we arbitrarily assume a value of $S_T = 20$ MPa, the Hashin matrix compression failure criterion (with nonlinear shear behavior) predicts a substantial increase in shear strength with moderate compressive stress, as shown in Figure 30. This example demonstrates that including the transverse shear strength in the matrix compression failure criterion has a significant effect on the strength of the composite under combined loading conditions if S_T is substantially less than S. However, we do not know if the transverse shear strength assumed in this example is appropriate. Rosen and Hashin in Reference [8] state that the transverse shear strength is difficult to measure. A reasonable approximation for S_T is the ultimate shear strength for the epoxy matrix alone, but the matrix shear strength was not reported in Reference [35].

Modified Tsai-Wu Failure Criterion.

Swanson and Christoforou in Reference [31] use an interactive failure criterion that is a modified form of the Tsai-Wu criterion. The criterion models both the transverse tensile and compressive behavior of carbon-epoxy. The quadratic criterion contains a linear term whose sign depends on the magnitude of the transverse tensile and compressive strengths, Y_T and Y_C, as follows:

$$F_2\sigma_{22} + F_{22}\sigma_{22}^2 + F_{66}\sigma_{12}^2 \geq 1 \tag{25}$$

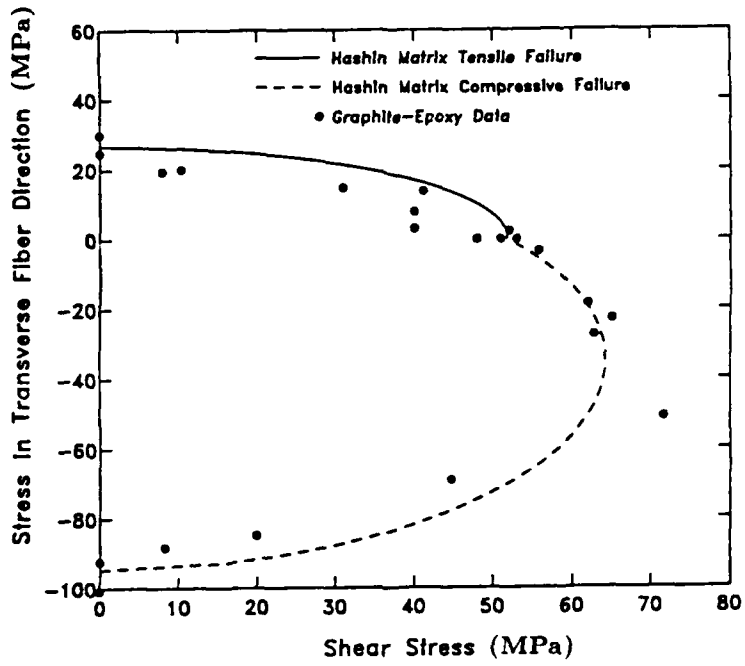

Figure 30. Comparison of Hashin matrix failure criteria with measured data for carbon-epoxy.

where

$$\begin{aligned} F_2 &= \frac{Y_C - Y_T}{Y_T Y_c} \\ F_{22} &= \frac{1}{Y_T Y_c} \\ F_{66} &= \frac{1}{S^2} \end{aligned} \tag{26}$$

This criterion fits the data very well, as is shown in Figure 31. Note that the criterion is obtained by neglecting all terms containing σ_{11} in Equation 2. The effect, if any, of σ_{11} on the matrix failure strength is an issue Swanson *et al.* in Reference [35] plan to address in future research.

Conclusions.

The Chang matrix criteria, the present criteria in DYNA3D, do not adequately model matrix failure observed in carbon-epoxy composites. When test data becomes available, additional studies should be performed on fiberglass-epoxy and Kevlar-epoxy composites of interest. Based on the studies completed to date, the modified Tsai-Wu criterion is recommended for modeling matrix tensile and compressive failure in fiber composites. Also, the modified Tsai-Wu criterion identifies the tensile and compressive matrix failure modes, continuing in the spirit of Chang to identify failure modes, so that progressive damage can be analyzed by including degradation of

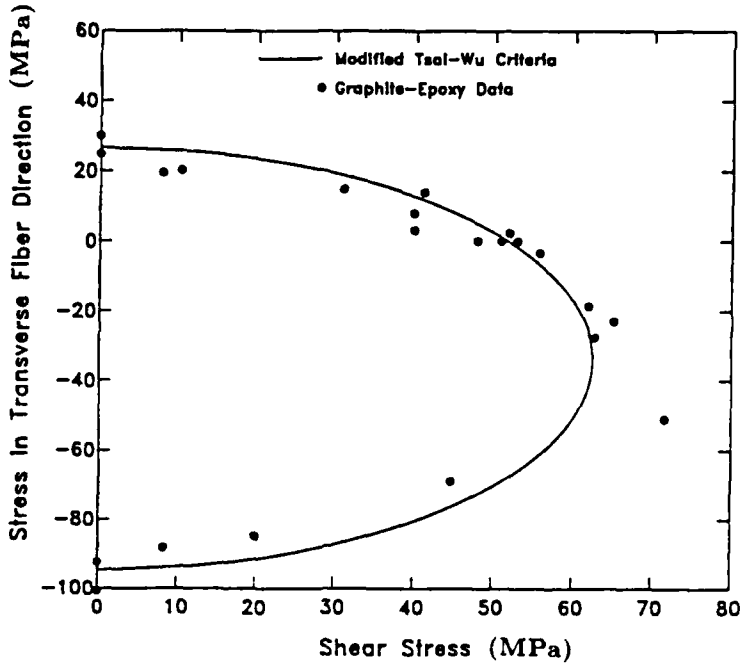

Figure 31. Comparison of modified Tsai-Wu criterion with matrix failure data for carbon-epoxy.

lamina properties.

Table 5. Failure criteria currently implemented in DYNA3D.

Failure Mode	Present Implementation	Recommended Implementation or Action
Fiber Tension	Chang Fiber Breakage	Verify Chang Fiber Breakage Criterion
Fiber Compression	None	Verify Interactive Criterion and Implement into DYNA3D
Matrix Tension	Chang Matrix Cracking	Implement Modified Tsai-Wu Criterion
Matrix Compression	Chang Matrix Compression	Implement Modified Tsai-Wu Criterion

2.3.4 Conclusions.

Table 5 compares the failure criteria currently implemented in DYNA3D with the criteria recommended for implementation. Based on comparisons of various failure criteria with test data available in the literature, the following conclusions are made:

- Comparisons of both the maximum fiber tensile stress criterion and the Chang fiber breakage criterion with carbon-epoxy data from biaxial stress tests were not conclusive in validating either criterion. This is because the maximum stress criterion, and the Chang fiber breakage criterion used in conjunction with a degraded shear modulus to account for matrix cracking, were both in reasonable agreement with the test data. However, the Tsai-Wu criterion was in poor agreement with the test data, which suggests that fiber failure is not adequately modeled by this criterion. Additional comparisons with test data are needed to validate the criteria, in particular the Chang fiber breakage criterion which is currently implemented in DYNA3D.

- Comparisons of both the maximum fiber compressive stress criterion and an interactive fiber compressive failure criterion with data from biaxial stress tests were not conclusive in validating either criterion. A fiber compressive failure criterion is not currently implemented in DYNA3D. Additional comparisons with test data are needed to validate a fiber compressive failure criterion for future implementation into DYNA3D.

- The modified Tsai-Wu criterion for matrix tensile and compressive failure is recommended for implementation into DYNA3D to replace the Chang matrix failure criteria. The modified Tsai-Wu criterion is in good agreement with failure strengths of carbon-epoxy measured under conditions of combined transverse-fiber and shear stress. The Chang matrix failure criteria are not in reasonable agreement with the test data. The Chang matrix tensile failure criterion overestimates the matrix tensile strength under combined load conditions. The Chang matrix compression failure criterion does not predict an increase in shear strength with moderate compressive stress comparable with that observed in the test data.

2.4 COMPARISON OF POST-FAILURE DEGRADATION RULES WITH EXPERIMENTAL RESULTS.

A number of post-failure material property degradation rules are available from the literature, see for example the survey by Nahas in Reference [17]. Many fit into one of three general categories: instantaneous unloading, gradual unloading, or constant stress after ply failure. These three categories were previously shown in Figure 14 of Section 2.2. Behavior of the ply when it unloads, as well as which elastic constants are degraded, depends on the mode of failure of the particular composite being analyzed.

One common method for estimating stiffness reductions in laminates with cracked plies is the *ply discount method.* With this method, one or more of the elastic constants of a cracked ply are set equal to zero. This method belongs to the instantaneous unloading category. For example, if matrix cracking failure occurs in a ply then the following are set to zero: Young's modulus in the transverse-fiber direction, E_{22}, the in-plane shear modulus, G_{12}, and the major and minor Poisson's ratio's, ν_{12} and ν_{21}. The ply is still able to carry longitudinal load in the fiber direction, *i.e.* $E_{11} \neq 0$. It is also assumed that degradation is restricted to the ply that cracks. The stiffness coefficients of the laminate are recalculated after the properties of the cracked ply are reduced. A ply discount scheme is presently implemented in DYNA3D.

Numerous studies are available from the literature for determining the stress-strain response of laminates with ply failure due to matrix cracking. Some of the earliest studies were done by Petit and Waddoups in Reference [38], who suggest a gradual failure model for boron-epoxy laminates, and Hahn and Tsai in Reference [39], who suggest a constant stress model for graphite-epoxy and glass-epoxy cross-ply laminates. More recent studies on transverse cracking and laminate stiffness reductions were performed by Talreja in Reference [40] and Highsmith and Reifsnider in Reference [41]. These studies are discussed in this section. Few studies are available for determining laminate stress-strain response in compression. Petit and Waddoups in Reference [38] suggest using a gradual failure model for ply matrix compression failure.

We begin this section with a description of matrix crack formation. This is followed by a discussion of results presented by Talreja, and Highsmith and Reifsnider, on stiffness-reduction mechanisms in cracked laminates. In the final section, modifications to the post-failure degradation rules currently implemented in DYNA3D are recommended.

2.4.1 Micromechanics of Matrix Cracking.

The initiation and subsequent multiplication of matrix cracks in transverse or off-axis plies of laminates subjected to longitudinal tension is presented in this section. Cracks initiate in transverse or off-axis plies at relatively low values of applied stress

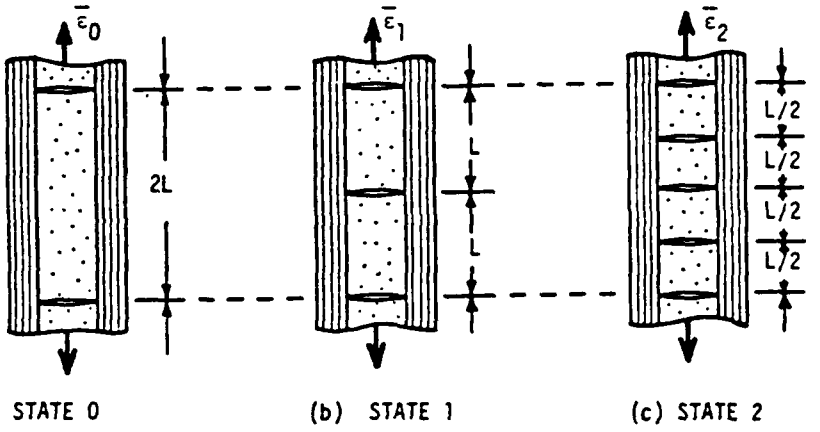

Figure 32. Multiplication of matrix cracks in the transverse ply of a laminate loaded in longitudinal tension.

or strain, 25% to 33% of the matrix fracture stress, as discussed in Reference [42]. Cracks initiate at areas where flaws exists or where fibers debond from the matrix. The initial cracks are widely spaced.

Nuismer and Tan, in Reference [43], developed a theoretical model in which crack multiplication proceeds in a deterministic manner. Consider a symmetric cross-ply laminate with an interior 90° ply (transverse to the applied strain) containing a periodic array of cracks of spacing 2L, as shown in Figure 32a. As the applied strain is slowing increased from $\bar{\epsilon}_0$ to $\bar{\epsilon}_1$, a new strain level is reached at which a new set of cracks is formed. The crack formation is assumed to be deterministic with the newly formed cracks equally spaced between the original cracks. This is reasonable because the transverse stress in the cracked lamina has a maximum value at these locations. The process continues as additional strain is applied, as shown in Figure 32c.

Reifsnider *et al.*, in Reference [42], suggest that when a matrix crack initiates, the load is transferred by adjacent plies back to the cracked ply over a distance which depends on the stiffness of the cracked and adjacent plies. A second crack will form in the cracked ply, at a distance away from the initial crack, when the failure stress of the matrix is exceeded. This process continues until the cracks reach an equilibrium or saturation state, commonly called the Characteristic Damage State (CDS). The saturated crack density is independent of the loading history but depends on the ply thicknesses, orientations, and stacking sequence, as discussed in Reference [44].

A number of studies are available which determine the stress or strain for the onset of cracking and the spacing between cracks, as discussed in References [43, 45]. Some studies, such as References [40, 41, 46], report the changes in laminate stiffness as well. Two studies on laminate stiffness reductions are discussed in the next two subsections.

2.4.2 Stress-Strain Behavior of Laminates with Matrix Cracking.

Studies on the stress-strain behavior of laminates with matrix cracks were performed by Talreja in Reference [40]. Talreja determined the reduction in longitudinal elastic moduli over the range from crack initiation to crack saturation and compared his predictions with experimental results for various glass-epoxy and graphite-epoxy laminates.

Consider a laminate consisting of arbitrarily oriented plies subjected to stress in the longitudinal direction (direction of 0° plies). The transverse or off-axis plies will develop matrix cracks. Talreja calls these plies 'cracking plies' and the remaining plies are called 'constraining plies'. Talreja determined that the initiation and development of transverse cracks are subject to constraints from two sources: the thickness of cracking plies and the stiffness of the constraining plies. Talreja reports that the strain for onset of matrix cracking decreases with increasing transverse ply thickness and increases with stiffness of the constraining plies.

Talreja uses a classification scheme to qualitatively assess laminate performance with cracking plies. The degree of constraint is classified into four types, as discussed in the following paragraphs. The laminate stress-strain behavior corresponding to these four types of constraints is shown schematically in Figures 33a to 33d.

Type A: No Constraint. The laminate stress-strain behavior corresponding to the limiting case of no constraint is shown in Figure 33a. The response is linear until the longitudinal strain reaches the failure strain of the cracking plies, ϵ_{FPF}, where FPF stands for first ply failure. The constraining plies are unable to carry the additional load shed by the cracking plies and extend instantaneously to failure, ϵ_c.

Type B: Low Constraint. The behavior of a low constraint laminate is shown in Figure 33b. Cracks initiate at a slightly higher strain than in Type A laminates. Once cracks initiate, the cracks multiply under constant load leading to an abrupt increase in strain. Further increases in load result in nonlinear stress-strain behavior due to the formation of additional cracks.

Type C: High Constraint. Figure 33c shows the stress-strain behavior for a high constraint laminate. Crack formation is represented by a knee in the stress-strain curve. Stable crack multiplication requires additional load increments. Negligible nonlinearity is observed due to the low increase in strain with matrix crack formation.

Type D: Full Constraint. Figure 33d shows the stress-strain behavior of a fully constrained laminate in which transverse cracks are fully suppressed. The laminate fails when the failure strain of the constraining plies is reached.

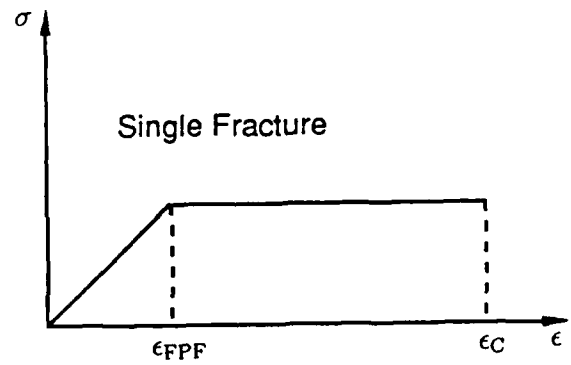

a. Type A: No Constraint.

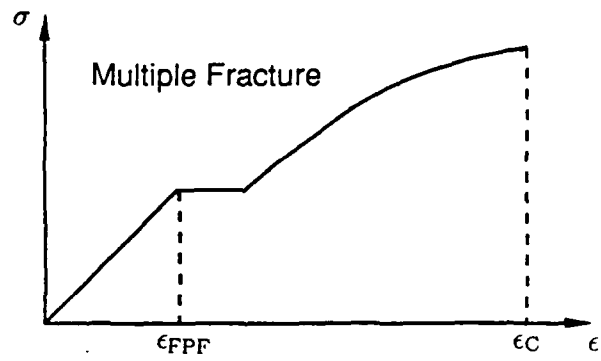

b. Type B: Low Constraint.

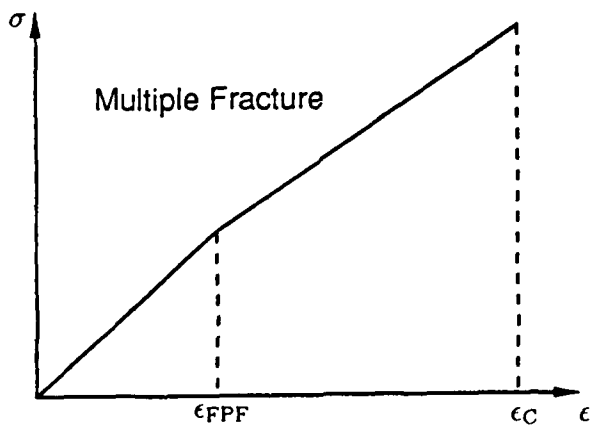

c. Type C: High Constraint.

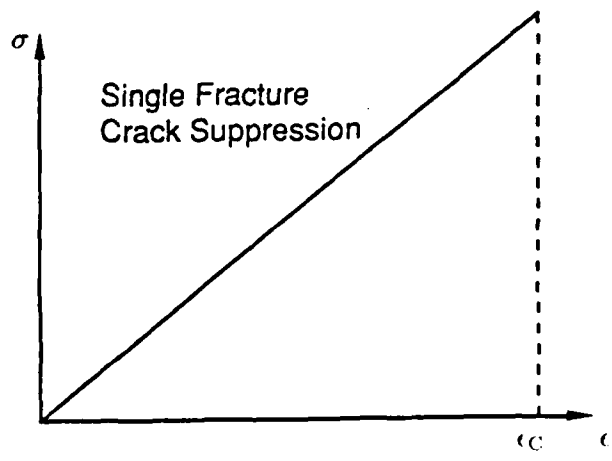

d. Type D: Full Constraint.

Figure 33. Effect of constraining ply stiffness on stress-strain behavior of laminates with cracking plies.

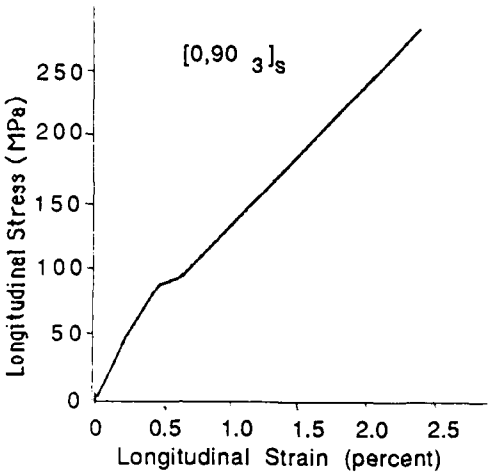

Figure 34. Longitudinal stress-strain diagram for a $[0°, 90°_3]_S$ glass-epoxy laminate.

Hahn and Tsai, in Reference [39], also suggest that the stress-strain behavior of laminates depends on whether the test is load controlled, as in Figure 33b, or displacement controlled. In a displacement controlled test, initiation and rapid multiplication of cracks would result in a drop in laminate stress at constant strain. This type of behavior was calculated with DYNA3D and previously shown in Figure 14.

Talreja compared the measured stress-strain behavior of laminates containing cracking plies with the behavior predicted from a damage mechanics theory[7]. Consider a symmetric cross-ply laminate, $[0°, 90°_3]_S$, made of glass-epoxy. The observed longitudinal stress-strain behavior for the laminate is shown in Figure 34. The behavior corresponds to the low constraint case, Type B. An abrupt increase in strain and subsequent drop in longitudinal modulus occur at 0.45% strain. The reduction in the longitudinal Young's modulus with applied stress is shown in Figure 35, where E_X and E_{X_0} are Young's moduli of the laminate with and without matrix cracking, respectively. The observed and predicted values agree quite well. Also shown in Figure 35 is the reduction in Young's modulus predicted with a ply discount scheme in which E_{22} and G_{12} of the cracked ply are set equal to zero. The prediction in Figure 35 based on the ply discount scheme overestimates the laminate modulus reduction by 12%.

Additional tests and analyses reported by Talreja indicate that the laminate stress-strain behavior and the reduction in laminate modulus depend on the particular layup.

[7]The predicted stress-strain behaviors were calculated by Talreja using a damage mechanics approach: the theory characterizes matrix damage by a vector field and he derives relationships between the laminate elastic moduli and magnitudes of the damage vectors. The damage vector is orientated normal to the plane of the crack. The magnitude of the damage vector depends on the crack density, average length and width of the crack, and a non-dimensional factor which depends on the constraint due to the finite thickness of the cracking plies. Material constants for the undamaged state and one damaged state (at a known crack density) must be measured. With his analysis, Talreja shows that an initially orthotropic solid becomes anisotropic as a result of matrix cracking.

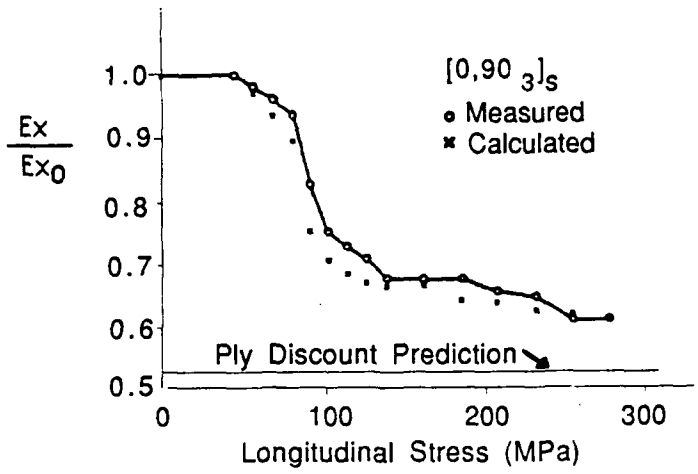

Figure 35. Reduction in longitudinal Young's modulus with applied longitudinal stress for a $[0°, 90°_3]_S$ glass-epoxy laminate.

For example, the behavior of the cross-ply laminate, $[0°, 90°]_S$, is characteristic of the high constraint case, Type C. This is because the alternating longitudinal plies provide a higher constraint to transverse cracking than those in the $[0°, 90°_3]_S$ laminate. The ply discount prediction overestimates the reduction in longitudinal Young's modulus by about 23%. As another example, Talreja characterizes a $[60°, 90°, -60°, 90°]_{2S}$ *laminate as approximately a no constraint-type laminate.* The ply discount method, with $E_{22} = 0$ and $G_{12} = 0$ in the 90° plies, underestimates the longitudinal modulus reduction by about 50%.

Talreja concluded that the ply discount scheme is unreliable for predicting minimum values of moduli for cracked laminates. He further concluded that the ply discount predictions tend to *overestimate* the longitudinal modulus reduction for high constraint cracking laminates and *underestimate* the reduction for low constraint cracking laminates. The alternating hoop and at-angle ply layups typically used in motor case design are probably high constraint type laminates.

Talreja's emphasis was on reduction in the longitudinal modulus of cracked laminates. A more thorough study was reported by Highsmith and Reifsnider in Reference [41] in which reductions in Poisson's ratio and shear modulus were also reported. Their results are briefly summarized in the next subsection.

2.4.3 Stiffness Reduction in Composite Laminates with Matrix Cracking.

Highsmith and Reifsnider, in Reference [41], reported results of quasi-static tension tests on four sets of glass-epoxy laminates. They obtained measurements of crack density and laminate stiffness verses applied longitudinal stress. Typical results for a $[0°, 90°_3]_S$ laminate are shown in Figure 36. The general trend is that as crack density increases, the stiffness decreases until both the crack density and laminate stiffness

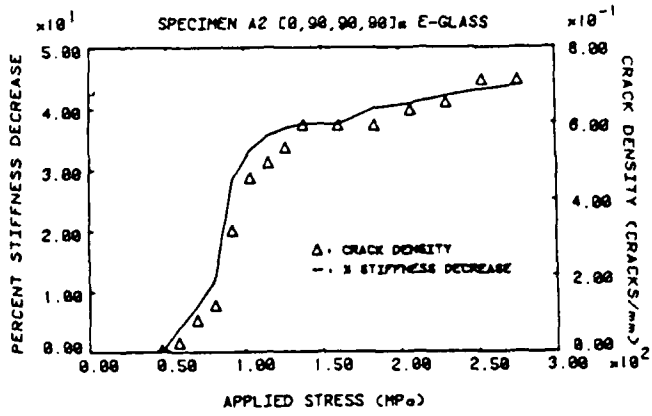

Figure 36. Crack density and laminate stiffness reduction versus applied longitudinal stress for a $[0°, 90°_3]_S$ laminate.

reach a stable value.

Measured reductions in laminate elastic constants, reported by Highsmith and Reifsnider, are compared in Table 6 with those calculated by APTEK with three ply discount schemes, where E_X is the laminate longitudinal modulus, ν_{XY} is the major Poisson's ratio, G_{XY} is the laminate in-plane shear modulus[8].

We begin discussion of Table 6 with results for the three cross-ply laminates. The comparative results indicate that all ply discount schemes overestimate the reduction in laminate modulus, E_X, for cross-ply laminates. The largest discrepancy is for the $[90°_3, 0°]_S$ laminate in which the stiffness reduction is overestimated by 22%. Significant reductions are observed in Poisson's ratio; all ply discount methods are in good agreement with the observed data for the cross-ply laminates. The measured results also indicate that that there is little (11.2%) or no reduction in laminate shear modulus for the cross-ply laminates. The ply discount scheme with G_{12} of the cracked ply set equal to zero is in poor agreement with the observed data. This suggests that it is not appropriate to discount the shear stiffness of cracked plies loaded in transverse tension.

For the laminate with 45° plies, none of the schemes are in good agreement with the measured data for E_X, ν_{XY} or G_{XY}. Highsmith and Reifsnider suggests that the agreement is not good because other damage modes were observed in this laminate, such as delaminations, longitudinal splitting, and fiber breakage.

2.4.4 Conclusions.

Tests and analyses results presented by Talreja, Highsmith and Reifsnider indicate that the reduction in ply properties with matrix cracking depends on the ply stacking sequence, ply stiffnesses, and cracking ply thickness. Thus, a general post-failure

[8]Highsmith and Reifsnider, in Reference [41], also reported the measured and predicted changes in laminate bending stiffness, D_{YY}.

Table 6. Measured and calculated reduction in elastic constants of glass-epoxy laminates. Property reductions are calculated with a ply discount method.

Laminate		Percent Reduction			Discounted Properties
		E_X	ν_{XY}	G_{XY}	
$[0, 90_3]_S$	Observed	42.0	—	0.0	
	Calculated	47.3	75.0	0.0	E_{22}
	Calculated	47.3	74.3	0.0	E_{22} ν_{12} ν_{21}
	Calculated	47.3	74.3	75.0	E_{22} ν_{12} ν_{21} G_{12}
$[90_3, 0]_S$	Observed	38.8	71.0	0.0	
	Calculated	47.3	75.0	0.0	E_{22}
	Calculated	47.3	74.3	0.0	E_{22} ν_{12} ν_{21}
	Calculated	47.3	74.3	75.0	E_{22} ν_{12} ν_{21} G_{12}
$[0, 90]_S$	Observed	17.1	49.8	11.2	
	Calculated	22.7	50.0	0.0	E_{22}
	Calculated	22.7	48.9	0.0	E_{22} ν_{12} ν_{21}
	Calculated	22.7	48.9	50.0	E_{22} ν_{12} ν_{21} G_{12}
$[0, \pm 45]_S$	Observed	9.4	8.1	28.4	
	Calculated	3.9	20.1	9.7	E_{22}
	Calculated	4.2	21.5	11.9	E_{22} ν_{12} ν_{21}
	Calculated	30.1	-29.4	11.9	E_{22} ν_{12} ν_{21} G_{12}

degradation rule must be implemented into DYNA3D that is capable of modeling ply stiffness reductions for arbitrarily stacked laminates. Allowing the user to specify the degradation behavior for each mode of failure would make the code more flexible. A flexible post-failure degradation model is suggested in the following paragraphs.

The post-failure degradation rules currently implemented in DYNA3D were discussed in Section 1.3.2. For the fiber breakage mode, all the lamina elastic constants (E_{11}, E_{22}, ν_{12}, ν_{21}, and G_{12}) are set to zero over an arbitrary number of time steps (100 time steps in the current version). For the matrix failure modes, some of the elastic constants are set to zero over a single time step.

The following changes to the current DYNA3D implementation are proposed:

1. Allow the user to specify the total strain increment over which property degradation occurs in each failure mode. The simplest model would be a linear degradation in elastic constants with strain. For example, if matrix cracking occurs at a uniaxial failure strain of ϵ_{crack}, the user might specify a reduction in E_{22}, ν_{12}, and ν_{21} over a total strain increment of $\epsilon_{\text{crack}}/4$. A small strain increment would produce nearly instantaneous unloading while a large strain increment would correspond to constant stress after ply failure.

2. Allow the user to specify the percent reduction in the lamina elastic constants for each failure mode. For example, if the user is analyzing a cross-ply laminate under longitudinal tension, the user might specify an 80% reduction in E_{22}, ν_{12}, and ν_{21}, and no reduction in G_{12}.

The suggested modifications allow the user to model constant stress, gradual unloading, or instantaneous unloading, following tensile or compressive failure of the fibers or matrix. Material property reductions as a function of strain are suggested because laminate stiffness reductions are generally reported in the literature as a function of applied stress or strain. An alternate implementation, to the first modification listed above, is to allow the user to specify the number of time steps over which property degradation occurs in each failure mode. The simplest model would be a linear degradation in elastic constants with each time step, as is currently implemented for the fiber breakage criterion. One difficultly with reducing the moduli over a specified number of time steps is that unloading behavior of the ply will not necessarily be linear with strain.

SECTION 3
LIST OF REFERENCES

1. Hallquist, J.O. and D.J. Benson, *DYNA3D User's Manual (Nonlinear Dynamic Analysis of Structures in Three Dimensions)*, Lawrence Livermore National Laboratory, Livermore CA, UCID-19582, Rev. 2, March 1986.

2. Hashin, Z., "Failure Criteria for Unidirectional Fiber Composites," *J. Applied Mechanics*, Vol. 47, June 1980, pp. 329-334.

3. Chang, F.K., and K.Y. Chang, "Post-Failure Analysis of Bolted Composite Joints in Tension or Shear-Out Mode Failure," *J. of Composite Materials*, Volume 21, pp. 809-833, 1987.

4. Chang, F., R. A. Scott and G. S. Springer, "Failure Strength of Nonlinearly Elastic Composite Laminates Containing a Pin Loaded Hole," *J. Composite Materials*, Vol. 18, Sept. 1984, pp. 464-477.

5. Chang, F.K., and K.Y. Chang, "A Progressive Damage Model for Laminated Composites Containing Stress Concentrations," *J. of Composite Materials*, Vol. 21, pp. 834-855, 1987.

6. Greszczuk et al., "Advanced Analysis and Design of Composite Materials and Structures," University of California, Los Angeles, Engineering 847.65 lecture notes, March 1989.

7. Smith, B.W., "Fractography for Continuous Fiber Composites," *Composites, Engineered Materials Handbook Volume 1,* ASM International Handbook Committee, Metals Park, Ohio, 1987, pp. 786-793.

8. Rosen, B.W., and Z. Hashin, "Analysis of Material Properties," *Composites, Engineered Materials Handbook Volume 1,* ASM International Handbook Committee, Metals Park, Ohio, 1987, pp. 185-205.

9. Rosen B.W., "Tensile Failure of Fibrous Composites," AIAA Journal, Volume 12, 1964, pp. 1982-1991.

10. Greszczuk, L.B., "On Failure Modes of Unidirectional Composites Under Compressive Loading," *Fracture of Composite Materials*, Proc. of Second USA-USSR Symposium, Bethlehem, PA, March 1981, pp. 231-244.

11. Greszczuk, L.B., "Microbuckling Failure of Circular Fiber-Reinforced Composites," AIAA Journal, Vol. 13, No. 10, October 1975, pp. 1311-1318.

12. Camponeschi, E. T. "Compression of Composite Materials: A Review," David Taylor Research Center, Bethesda, MD 20084, AD-A189 272, 1988.

13. Yeh, J.R., and J.L. Teply, "Compressive Response of Kevlar/Epoxy Composites," *J. of Composite Materials*, Vol. 22, March 1988, pp. 245-257.

14. Burk, R. C., "Standard Failure Criteria Needed for Advanced Composites," *Astronautics and Aeronautics*, Vol. 21, June 1983, pp. 58-62.

15. Hill, R., *The Mathematical Theory of Plasticity*, Oxford University Press, London, 1950.

16. Tsai, S. W., and V. D. Azzi, "Strength of Laminated Composite Materials," *AIAA Journal*, Vol. 4, No. 2, Feb. 1966, pp. 296-301.

17. Nahas, M. N., "Survey of Failure and Post-Failure Theories of Laminated Fiber-Reinforced Composites," *J. Composites Technology & Research*, Vol. 8, No. 4, Winter 1986, pp. 138-153.

18. Tsai, S. W., and E. M. Wu, "A General Theory of Strength for Anisotropic Materials," *J. Composite Materials*, Vol. 5, Jan. 1971, pp. 58-80.

19. Tsai, S. W., and H. T. Hahn, "Failure Analysis of Composite Materials," *Inelastic Behavior of Composite Materials*, ASME, AMD-Vol. 13, 1975, pp. 73-96.

20. Rowlands, R. E., "Flow and Failure of Biaxially Loaded Composites: Experimental - Theoretical Correlation," *Inelastic Behavior of Composite Materials*, ASME, AMD-Vol. 13, 1975, pp. 97-125.

21. Yamada, S. E., and C. T. Sun, "Analysis of Laminate Strength and its Distribution," *J. Composite Materials*, Vol. 12, July 1978, pp. 275-284.

22. Sandhu, R. S., "Nonlinear Behavior of Unidirectional and Angle-Ply Laminates," *Journal of Aircraft*, Vol.13, Feb. 1974, pp. 104-111.

23. Hahn, H. T., and S. W. Tsai, "Non-linear Behavior of Unidirectional Composite Lamina," *J. Composite Materials*, Vol. 7, Jan. 1973, pp. 102-118.

24. Simo, J., "Some Aspects of Continuum Damage Mechanics and Strain Softening", Department of Mechanical Engineering, Stanford University, Stanford, CA.1988.

25. Guess, T.R., "Kevlar/Epoxy Laminates: Mechanical Response of As-Fabricated and Shock-Loaded Materials," Sandia National Laboratories, Albuquerque, NM, SAND87-0620, June 1987.

26. Zweben, C., "The Flexural Strength of Aramid Fiber Composites," *J. of Composite Materials*, Vol. 12, Oct. 1978, p. 422.

27. Jang, J., "Numerical Simulation of Inplane Damage in Thin Composite Structures," Department of Mechanical Engineering, Stanford University, Stanford, CA, 1988.

28. Murray, Y.D. *Fibrous Composite Laminates: An Introduction to the Theory, and Verification of the DYNA3D Implementation*, APTEK, Inc., San Jose, CA., DNA-TR-88-191, August 1988.

29. Foral, R.F. "Local Damage Effects on Performatnce of Filament Wound Composite Tubes," *Mechanics of Composite Materials*, AMD-Vol. 92, 1988, pp. 135-142.

30. Carlsson, L.A., and R. Byron Pipes, *Experimental Characterization of Advanced Composite Materials,* Prentice-Hall Inc., Englewood Cliffs, New Jersey 07632.

31. Swanson, S.R., and A.P. Christoforou, "Progressive Failure in Carbon/Epoxy Laminates Under Biaxial Stress", *J. of Engineering Materials and Technology*, January 1987, Vol. 109, pp. 12-16.

32. Swanson, S.R., and A.P. Christoforou, "Response of Quasi-Isotropic Carbon/Epoxy Laminates to Biaxial Stress," *J. of Composite Materials*, Vol. 20. September 1986, pp. 457-471.

33. Swanson, S.R., and M. Nelson, "Failure Properties of Carbon/Epoxy Laminates Under Tension-Compression Biaxial Stress," 1986, Proc. 3rd Japan-U.S. Conf. on Composite Materials, Tokyo, pp. 279-286.

34. Christensen, R.M., and S.R. Swanson, "Evaluation of a New Failure Criterion for Fibrous Composite Materials," *Mechanics of Composite Materials*, AMD-Vol. 92, 1988, pp. 63-68.

35. Swanson, S.R., M. Messick, and Z. Tian, "Failure of Carbon/Epoxy Lamina Under Combined Stress", *J. of Composite Materials*, 21, 1988, pp. 619-630.

36. ASM Committe on Forms and Properties of Composite Materials, "High-Strength Medium-Temperature Thermoset Matrix Composites," *Composites, Engineered Materials Handbook Volume 1,* ASM International Handbook Committee, Metals Park, Ohio, 1987, pp. 399-415.

37. Humphreys, E.A., and B. W. Rosen, "Property Analysis of Laminates," *Composites, Engineered Materials Handbook Volume 1,* ASM International Handbook Committee, Metals Park, Ohio, 1987, pp. 218-235.

38. Petit, P.H., and M.E. Waddoups, "A Method of Predicting the Nonlinear Behavior of Laminated Composites," *J. of Composite Materials*, Vol. 3, Jan 1969, pp. 2-19.

39. Hahn, H.T., and S.W. Tsai, "On the Behavior of Composite Laminates After Initial Failures," *J. of Composite Materials*, Vol. 8, July 1974, pp. 288-305.

40. Talreja, R., "Transverse Cracking and Stiffness Reduction in Composite Laminates," *J. of Composite Materials*, Vol. 19, July 1985, pp. 355-375.

41. Highsmith, A.L., and K.L. Reifsnider, "Stiffness-Reduction Mechanisms in Composite Laminates," *Damage in Composite Materials*, ASTM STP 775, American Society for Testing and Materials, Philadelphia PA, pp. 103-117.

42. Reifsnider, K.L., E.G. Henneke, W.W. Stinchcomb, and J.C. Duke, "Damage Mechanics and NDE of Composite Laminates," *Mechanics of Composite Materials. Recent Advances,* Pergamon, 1983, pp. 399-418.

43. Nuismer, R.J., and S.C. Tan, "The Role of Matrix Cracking in the Continuum Constitutive Behavior of a Damaged Composite Ply," *Mechanics of Composite Materials, Recent Advances,* Pergamon, 1983, pp. 437-448.

44. Masters, J.E., and K.L. Reifsnider, "An Investigation of Cumulative Damage Development in Quasi-Isotropic Graphite/Epoxy Laminates," *Damage in Composite Materials,* ASTM STP 775, American Society for Testing and Materials, Philadelphia PA, pp. 40-62.

45. Crossman, F.W., and A.S.D. Wang, "The Dependence of Transverse Cracking and Delamination on Ply Thickness in Graphite/Epoxy Laminates," *Damage in Composite Materials,* ASTM STP 775, American Society for Testing and Materials, Philadelphia PA, pp. 118-139.

46. Dvorak, G.J., N. Laws, and M. Hejazi, "Analysis of Progressive Matrix Cracking in Composite Laminates I. Thermoelastic Properties of a Ply with Cracks," *J. of Composite Materials,* Vol. 19, May 1985, pp. 216-234.

DISTRIBUTION LIST

DNA-TR-89-132

DEPARTMENT OF DEFENSE

DEFENSE ADVANCED RSCH PROJ AGENCY
ATTN: F PATTEN

DEFENSE INTELLIGENCE AGENCY
ATTN: RTS-2B

DEFENSE NUCLEAR AGENCY
ATTN: SPSD
ATTN: SPWE MAJ WOLF
4 CYS ATTN: TITL

DEFENSE TECHNICAL INFORMATION CENTER
2 CYS ATTN: DTIC/FDAB

STRATEGIC DEFENSE INITIATIVE ORGANIZATION
ATTN: T/KT LTCOL MARTIN

UNDER SECRETARY OF DEFENSE
ATTN: J PERSCH

DEPARTMENT OF THE ARMY

U S ARMY MATERIAL TECHNOLOGY LABORATORY
ATTN: R FITZPATRICK

U S ARMY STRATEGIC DEFENSE COMMAND
ATTN: SDC/E MONTGOMERY

DEPARTMENT OF THE NAVY

NAVAL RESEARCH LABORATORY
ATTN: CODE 4600 D NAGEL

DEPARTMENT OF THE AIR FORCE

AIR FORCE CTR FOR STUDIES & ANALYSIS
ATTN: AFCSA/SAMI R GRIFFIN

FOREIGN TECHNOLOGY DIVISION, AFSC
ATTN: TQX-1, J TUSS

WEAPONS LABORATORY
ATTN: NTC C AEBY
ATTN: TA LT COL W MULZER
ATTN: TA LT COL HERRERA
ATTN: TALE T EDWARDS
ATTN: TAS MAJ SQUILLER

WRIGHT RESEARCH & DEVELOPMENT CENTER
ATTN: MLPJ J RHODEHAMEL
ATTN: MLP W WOODY
ATTN: MLPJ R RONDEAU

DEPARTMENT OF ENERGY

LAWRENCE LIVERMORE NATIONAL LAB
ATTN: F SERDUKE
ATTN: L-84 H KRUGER
ATTN: M GERRISSIMENRO

LOS ALAMOS NATIONAL LABORATORY
ATTN: B259 A GREENE
ATTN: C931 T KING
ATTN: E548 R S DINGUS

SANDIA NATIONAL LABORATORIES
ATTN: DIV 8242 M BIRNBAUM

SANDIA NATIONAL LABORATORIES
ATTN: K MATZEN
ATTN: ORG 1230 J E POWELL

DEPARTMENT OF DEFENSE CONTRACTORS

AEROSPACE CORP
ATTN: H BLAES M2-250
ATTN: R COOPER
ATTN: T PARK

APTEK, INC
2 CYS ATTN: DR E FITZGERALD
ATTN: DR S SUTHERLAND
2 CYS ATTN: Y D MURRAY

BATTELLE MEMORIAL INSTITUTE
ATTN: C WALTERS

GENERAL RESEARCH CORP
ATTN: R PARISSE

JAYCOR
ATTN: M TREADAWAY

KAMAN SCIENCES CORP
ATTN: N FERRITER
ATTN: R ALMASSY

KAMAN SCIENCES CORPORATION
ATTN: DASIAC

KAMAN SCIENCES CORPORATION
ATTN: DASIAC

KTECH CORP
ATTN: D KELLER

MCDONNELL DOUGLAS CORPORATION
ATTN: J S KIRBY
ATTN: L COHEN
ATTN: L THOMPSON

MORTON THIOKOL, INC.
ATTN: D BAKER

PACIFIC-SIERRA RESEARCH CORP.
ATTN: H BRODE

PHYSICAL SCIENCES, INC.
ATTN: M MILLER

PHYSICS INTERNATIONAL CO.
ATTN: R RODENBERG

R & D ASSOCIATES
ATTN: B GOULD
ATTN: D GAKENHEIMER
ATTN: P A MILES

S-CUBED
ATTN: G GURTMAN

SCIENCE APPLICATIONS INTL CORP.
ATTN: E TOTON

SRI INTERNATIONAL
ATTN: B HOLMES
ATTN: D CURRAN
ATTN: G ABRAHAMSON